

# CHEMISTRY

## A European Journal

A Journal of



### Accepted Article

**Title:** Homometallic DyIII Complexes of Varying Nuclearity from 2 to 21: Synthesis, Structure and Magnetism

**Authors:** Vadapalli Chandrasekhar, Sourav Biswas, Sourav Das, Joydev Acharya, Vierandra Kumar, Jan Leusen, Juan Manuel Herrera, Paul Koegerler, and Enrique Colacio

This manuscript has been accepted after peer review and appears as an Accepted Article online prior to editing, proofing, and formal publication of the final Version of Record (VoR). This work is currently citable by using the Digital Object Identifier (DOI) given below. The VoR will be published online in Early View as soon as possible and may be different to this Accepted Article as a result of editing. Readers should obtain the VoR from the journal website shown below when it is published to ensure accuracy of information. The authors are responsible for the content of this Accepted Article.

**To be cited as:** *Chem. Eur. J.* 10.1002/chem.201700471

**Link to VoR:** <http://dx.doi.org/10.1002/chem.201700471>

Supported by  
**ACES**

WILEY-VCH

# Homometallic Dy<sup>III</sup> Complexes of Varying Nuclearity from 2 to 21: Synthesis, Structure and Magnetism

*Sourav Biswas,<sup>a</sup> Sourav Das,<sup>b</sup> Joydev Acharya,<sup>a</sup> Vierandra Kumar,<sup>a</sup> Jan van Leusen,<sup>c</sup> Paul Kögerler<sup>\*c</sup>, Juan Manuel Herrera,<sup>d</sup> Enrique Colacio<sup>\*d</sup> and Vadapalli Chandrasekhar<sup>\*a,e</sup>*

<sup>a</sup>Department of Chemistry, Indian Institute of Technology Kanpur, Kanpur-208016, India.

<sup>b</sup>Department of Chemistry, Institute of Infrastructure Technology Research and Management, Ahmedabad-380026, India.

<sup>c</sup>Institut für Anorganische Chemie, RWTH Aachen University, D-52074 Aachen, Germany.

<sup>d</sup>Departamento de Química Inorganica, Facultad de Ciencias, Universidad de Granada, 18071 Granada, Spain

<sup>e</sup>National Institute of Science Education and Research, Institute of Physics Campus, Sachivalaya Marg, PO: Sainik School, Bhubaneswar - 751 005, India

AUTHOR EMAIL ADDRESS: vc@iitk.ac.in; paul.koegerler@ac.rwth-aachen.de;

ecolacio@ugr.es

## Abstract

The synthesis, structure and magnetic properties of the four Dy(III) coordination compounds isolated as  $[\text{Dy}_2(\text{LH}_2)_2(\mu_2\text{-}\eta^1\text{:}\eta^1\text{-Piv})]\text{Cl}\cdot 2\text{MeOH}\cdot \text{H}_2\text{O}$  (**1**),  $[\text{Dy}_4(\text{LH})_2(\mu_3\text{-OH})_2(\text{Piv})_4(\text{MeOH})_2]\cdot 4\text{MeOH}\cdot 2\text{H}_2\text{O}$  (**2**),  $[\text{Dy}_6(\text{LH}_2)_3(\text{tfa})_3(\text{O}_3\text{P}^t\text{Bu})(\text{Cl})_3]\text{Cl}_4\cdot 15.5\text{H}_2\text{O}\cdot 4\text{MeOH}\cdot 5\text{CHCl}_3$  (**3**) and  $[\text{Dy}_{21}(\text{L})_7(\text{LH})_7(\text{tfa})_7]\text{Cl}_7\cdot 15\text{H}_2\text{O}\cdot 7\text{MeOH}\cdot 12\text{CHCl}_3$  (**4**) are reported (Piv = pivalate, tfa = 1,1,1-trifluoro-acetylacetone,  $\text{O}_3\text{P}^t\text{Bu}$  = *tert*-butylphosphonate). These compounds are accomplished through fine interplay between keto-enol tautomerism of a multidentate flexible ligand, 6-((bis(2-hydroxyethyl)amino)methyl)-*N'*-((8-hydroxyquinolin-2-yl)methylene)picolinohydrazide ( $\text{LH}_4$ ), triggered by stepwise deprotonation. Some of these polynuclear coordination complexes exhibit aesthetic and unprecedented structural features. Thus, complex **3** displays an equilateral triangle topology with side length of 9.541 Å and a rare pentagonal-bipyramidal  $\text{Dy}^{3+}$  environment, while complex **4** exhibits a single-stranded nanowheel structure with highest nuclearity known for a homometallic lanthanide cluster structure. A tentative model of the dc magnetic susceptibility and the low-temperature magnetization of compounds **1** and **2** indicates that the former exhibits weak ferromagnetic intramolecular exchange interaction between the  $\text{Dy}^{3+}$  ions, whereas in the latter both intramolecular ferromagnetic and antiferromagnetic magnetic exchange interactions are present. Compounds **1**, **3** and **4** exhibit frequency-dependent ac signals below 15 K at zero bias field, but without exhibiting any maximum above 2 K at frequencies up to 1400 Hz. The observed slow relaxation of the magnetization suggests that these compounds could exhibit SMM behavior with either a thermal energy barrier for the reversal of the magnetization that is not high enough to block the magnetization above 2 K or there exists quantum tunneling of the magnetization

(QTM). The very small energy separation between the ground and first excited states extracted for **1** and **2** from the magnetic data are in good agreement with the above hypothesis.

**Keyword:** polynuclear lanthanide compound, hexanuclear assembly, Schiff base, butterfly complex, equilateral triangle, macrocycle, anisotropy, energy barrier, ac susceptibility, slow magnetic relaxation.

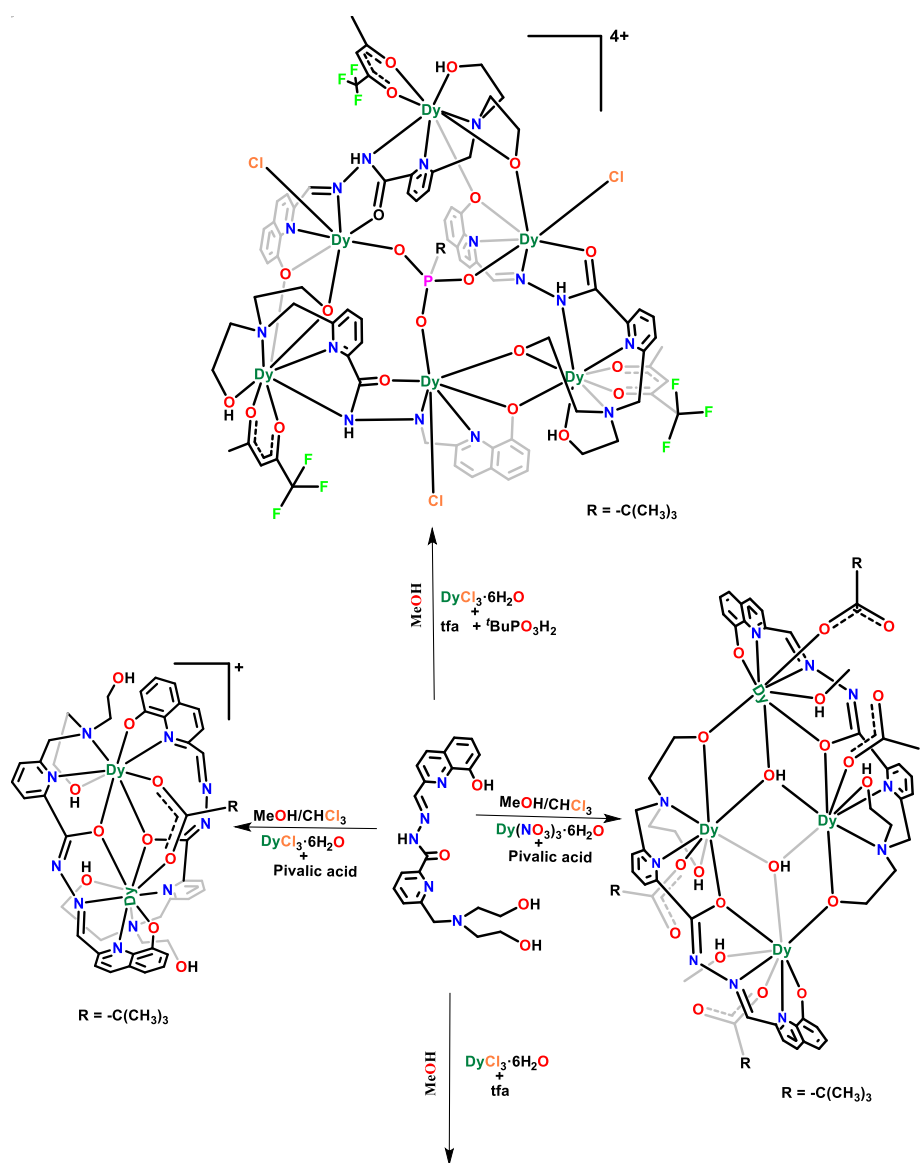
## Introduction

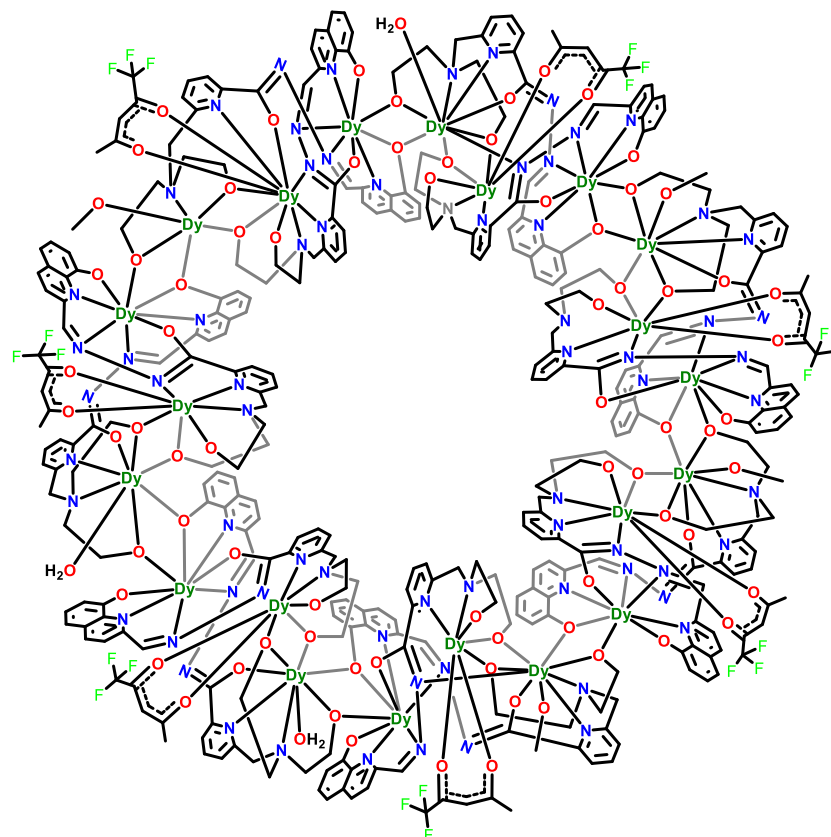
Synthesis and studies of molecular magnets have attracted considerable interest for about two decades, particularly since the discovery of single-molecule magnet (SMM) behavior in  $[\text{Mn}^{\text{IV}}_4\text{Mn}^{\text{III}}_8(\mu_3\text{-O})_{12}(\text{O}_2\text{CMe})_{16}(\text{OH}_2)_4]\cdot 2\text{MeCO}_2\text{H}\cdot 4\text{H}_2\text{O}$ .<sup>[1]</sup> A wide range of approaches have been explored in order to identify novel members of the family of single-molecule magnets.<sup>[2]</sup> The types of complexes investigated include 3d/4f complexes,<sup>[3]</sup> polynuclear transition metal complexes<sup>[4]</sup> as well as homonuclear 4f complexes<sup>[2a-c,5]</sup>. Recently heavier transition metal ion<sup>[6]</sup> as well as actinide<sup>[7]</sup> complexes are also being investigated. All of these strategies aim to achieve a high ground-state spin for the complex along with a significant magnetic anisotropy. Both theoretical and experimental investigations have revealed that the energy barrier of the double-well potential in SMMs is governed by both the total spin of the complex along with the magnetic anisotropy.<sup>[8]</sup> Among lanthanides,  $\text{Dy}^{3+}$  has been a natural choice of investigation since it is a Kramer's ion and can possess large single-ion magnetic anisotropy.<sup>[8]</sup> Accordingly, several  $\text{Dy}^{\text{III}}$  complexes have and continue to be investigated.<sup>[2a,b,5]</sup> One of the points of interest for a synthetic chemist has been the capability to modulate the nuclearity of complexes by a subtle control exercised by the choice of ligands. Most often, it has been noticed that one type of ligand generally affords a particular type of complex possessing a certain nuclearity and topology.<sup>[9]</sup> In this regard, we have been interested to investigate and ascertain if a given ligand under slightly varying conditions can enable the assembly of complexes with varying nuclearity and topology. Towards this end, we have designed a new multidentate, flexible, aroyl hydrazone-based Schiff base ligand, 6-((bis(2-hydroxyethyl)amino)methyl)-*N'*-((8-hydroxyquinolin-2-yl)methylene)picolinohydrazide ( $\text{LH}_4$ ), with which we have been able to assemble the coordination compounds  $[\text{Dy}_2(\text{LH}_2)_2(\mu_2\text{-}\eta^1\text{:}\eta^1\text{-Piv})]\text{Cl}\cdot 2\text{MeOH}\cdot \text{H}_2\text{O}$  (**1**),  $[\text{Dy}_4(\text{LH})_2(\mu_3\text{-}$



$[\text{Dy}_{21}(\text{L})_7(\text{LH})_7(\text{tfa})_7]\text{Cl}_7 \cdot 15\text{H}_2\text{O} \cdot 7\text{MeOH} \cdot 12\text{CHCl}_3$  (4) (Scheme 1). Interestingly, depending on the reaction conditions, the metal nuclearity of the obtained complexes varies from 2 to 21.

Herein, we report the synthesis, structure and magnetism of the complexes 1–4.





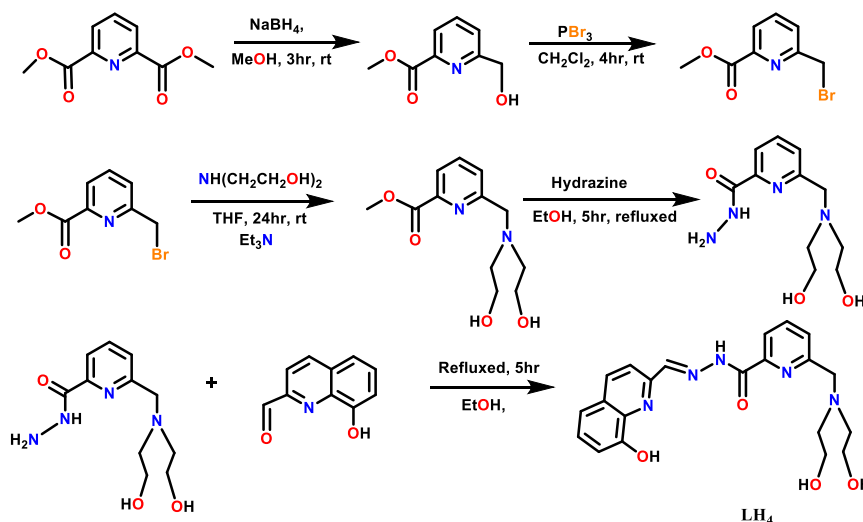
**Scheme 1.** Formation of Dy<sub>2</sub>, Dy<sub>4</sub>, Dy<sub>6</sub> and Dy<sub>21</sub> assemblies using LH<sub>4</sub>.

## Result and Discussion

### Synthetic Aspects

We have been involved in the design and utilization of various types of ligand families for the preparation of 3d/4f<sup>[3g-i,9d,f]</sup> and 4f<sup>[2e,5a-d,f,i,j,9a,g]</sup> complexes. From our experience<sup>[2e,5a,j,f,9i]</sup> and those of others<sup>[2f,10]</sup> we have observed that flexible ligands that have multiple options to bind to a metal ion are often suitable to generate polynuclear complexes. Among the ligands that we have investigated, aroyl hydrazone ligands have been found to possess the following beneficial

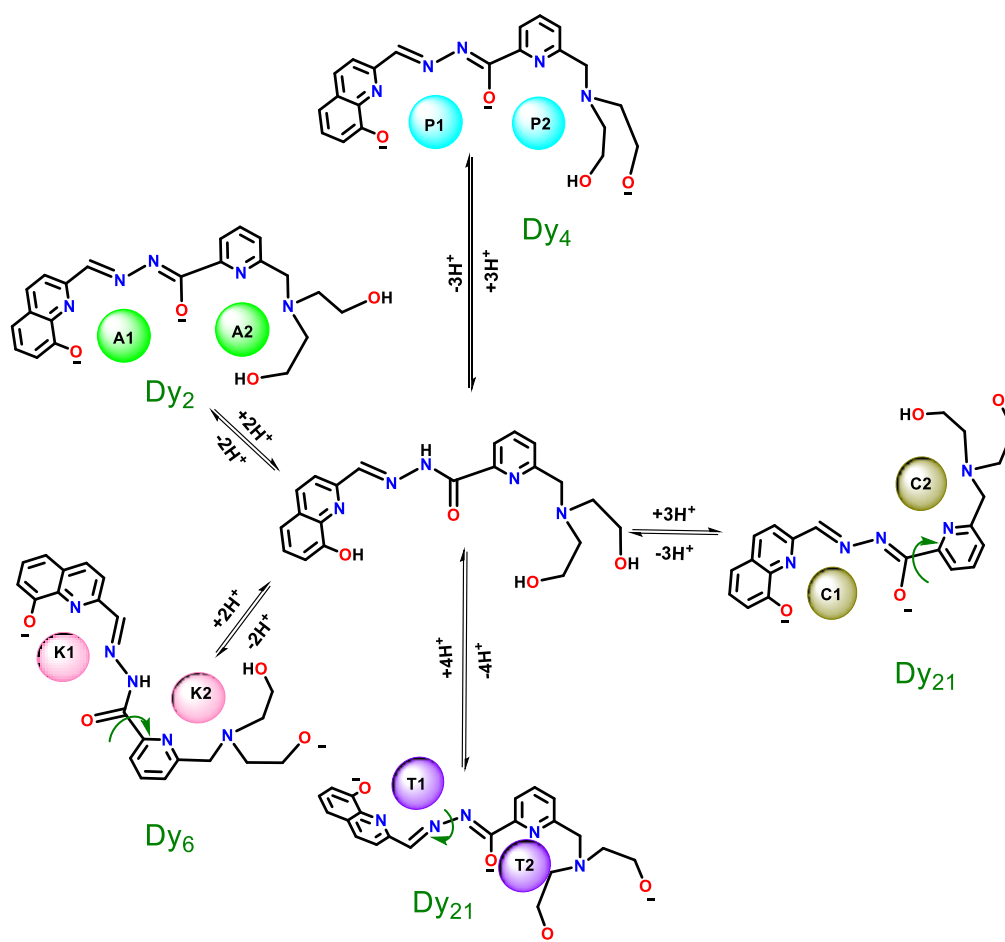
features. Firstly, these ligands can exhibit keto–enol tautomerism whereby the enolate/neutral forms can be involved in binding. Secondly, the presence of C–C bond rotation in this family of ligands allows the presence of conformational isomers of different coordinating capabilities.<sup>[9g, 10b-d]</sup> Accordingly, we designed and synthesized a new multidentate flexible aroyl hydrazone based Schiff base ligand, LH<sub>4</sub>, as shown in Scheme 2.



**Scheme 2.** Synthesis of LH<sub>4</sub>.

The ligand LH<sub>4</sub> contains nine divergent coordination sites that can be partitioned into two pockets in five different ways depending upon the deprotonation level. The observed coordination behavior in the current instance can be summarized for the ligand in three different possibilities. First, at the double deprotonation level the ligand can behave in two different ways: in the enol form, [LH<sub>2</sub>]<sup>2-</sup> generates two tetradentate pockets with identical O<sub>2</sub>N<sub>2</sub> coordination environments (A1 and A2), while in the keto form, due to C–C bond rotation, two pockets N<sub>3</sub>O<sub>2</sub> (K2) and O<sub>2</sub>N<sub>2</sub> (K1) result, which are oriented in opposite directions. Second, at the triple deprotonation level, [LH]<sup>3-</sup> (enol form), pockets P1 and P2 are tetradentate (O<sub>2</sub>N<sub>2</sub>) and

pentadentate ( $O_3N_2$ ), respectively, and are oriented in the same direction, while pockets C1 ( $O_2N_2$ ) and C2 ( $N_3O_2$ ) are projected in the opposite direction as a result of C–C bond rotation. Third, at the tetra-deprotonation level, an unprecedented N–N bond rotation enables the formation of two asymmetric pockets, T1 ( $ON_2$ ) and T2 ( $O_3N_2$ ), which are oriented nearly perpendicular to each other. These coordination modes and the nuclearities of the different types of the resulting complexes are summarized in Scheme 3.



**Scheme 3.**  $LH_4$  showing two coordination pockets in various conformations.

The reaction of  $LH_4$ ,  $DyCl_3$  and pivalic acid in the presence of  $Et_3N$  in a stoichiometric ratio of 2:2:1:6 afforded a dinuclear complex, isolated as  $[Dy_2(LH_2)_2(\mu_2-\eta^1:\eta^1-Piv)]Cl \cdot 2MeOH \cdot 2H_2O$  (**1**).

On the other hand, the reaction of  $\text{LH}_4$ ,  $\text{Dy}(\text{NO}_3)_3 \cdot 6\text{H}_2\text{O}$  and pivalic acid in the presence of  $\text{Et}_3\text{N}$  with a stoichiometric ratio of 1:2:2:6 under refluxing conditions fostered the formation of a charge-neutral homometallic tetranuclear complex,  $[\text{Dy}_4(\text{LH})_2(\mu_3\text{-OH})_2(\text{Piv})_2(\text{MeOH})] \cdot 4\text{MeOH} \cdot \text{H}_2\text{O}$  (**2**) (Scheme 1). Changing the co-ligand from pivalic acid to 1,1,1-trifluoroacetyl acetone and utilizing *tert*-butyl phosphonic acid afforded the hexanuclear complex  $[\text{Dy}_6(\text{LH}_2)_3(\text{tfa})_3(\text{O}_3\text{P}^t\text{Bu})(\text{Cl})_3]\text{Cl}_4 \cdot 15.5\text{H}_2\text{O} \cdot 4\text{MeOH} \cdot 5\text{CHCl}_3$  (**3**). A further change in stoichiometry and reaction conditions (see experimental section) yielded a macrocyclic complex, isolated as  $[\text{Dy}_{21}(\text{L})_7(\text{LH})_7(\text{tfa})_7]\text{Cl}_7 \cdot 15\text{H}_2\text{O} \cdot 7\text{MeOH} \cdot 12\text{CHCl}_3$  (**4**). Note that apart from the role played by the primary ligand in the formation of the complexes, the co-ligands, namely pivalic acid (for **1** and **2**), trifluoroacetyl acetone and *tert*-butyl phosphonic acid (for **3**) and trifluoroacetyl acetone acid (for **4**) assist the formation of the molecular complexes by providing the additional binding that is needed to meet the  $\text{Dy}^{3+}$  coordination requirements. In addition, the crucial capping coordination role of the phosphonate ligand in the formation of **3** is readily noted. It seems likely that the coordination flexibility of the ligand (as a result of variable deprotonation ability, keto-enol tautomerism, rotation around C-C and N-N bond) along with the subtle influence of the co-ligand(s) allows the modulation of nuclearity among the homometallic complexes. While the variation of nuclearity of the complexes was achieved through trial and error, we hope that such endeavors are a step forward towards rational synthetic pathways for achieving desired nuclearities.

In order to check the structural integrity of these complexes in solution, we have carried out ESI-MS studies. These reveal for **1**, **2**, and **3** respectively, peaks at  $m/z = 1139.191$ ,  $1902.299$  and  $1474.066$  corresponding to the species  $[\text{C}_{47}\text{H}_{51}\text{Dy}_2\text{N}_{10}\text{O}_{10} - \text{Piv} - \text{H}^+]^+$ ,  $[\text{C}_{64}\text{H}_{86}\text{Dy}_4\text{N}_{10}\text{O}_{20} - 2\text{MeOH} + \text{H}^+]^+$  and  $[\text{C}_{82}\text{H}_{81}\text{Cl}_3\text{Dy}_6\text{F}_9\text{N}_{15}\text{O}_{21}\text{P} - 2\text{Cl}^- + 3\text{H}_2\text{O} + 2\text{MeOH} - 4\text{H}^+]^{2+}$ . This indicates that

these complexes remain partially intact in solution. In contrast, **4** seems to fragment completely in solution. A perspective view of the ESI-MS spectra of complex **1** is given in Figure 1 and that of **2** and **3** are compiled in the Supporting Information (Figures S1 and S2).

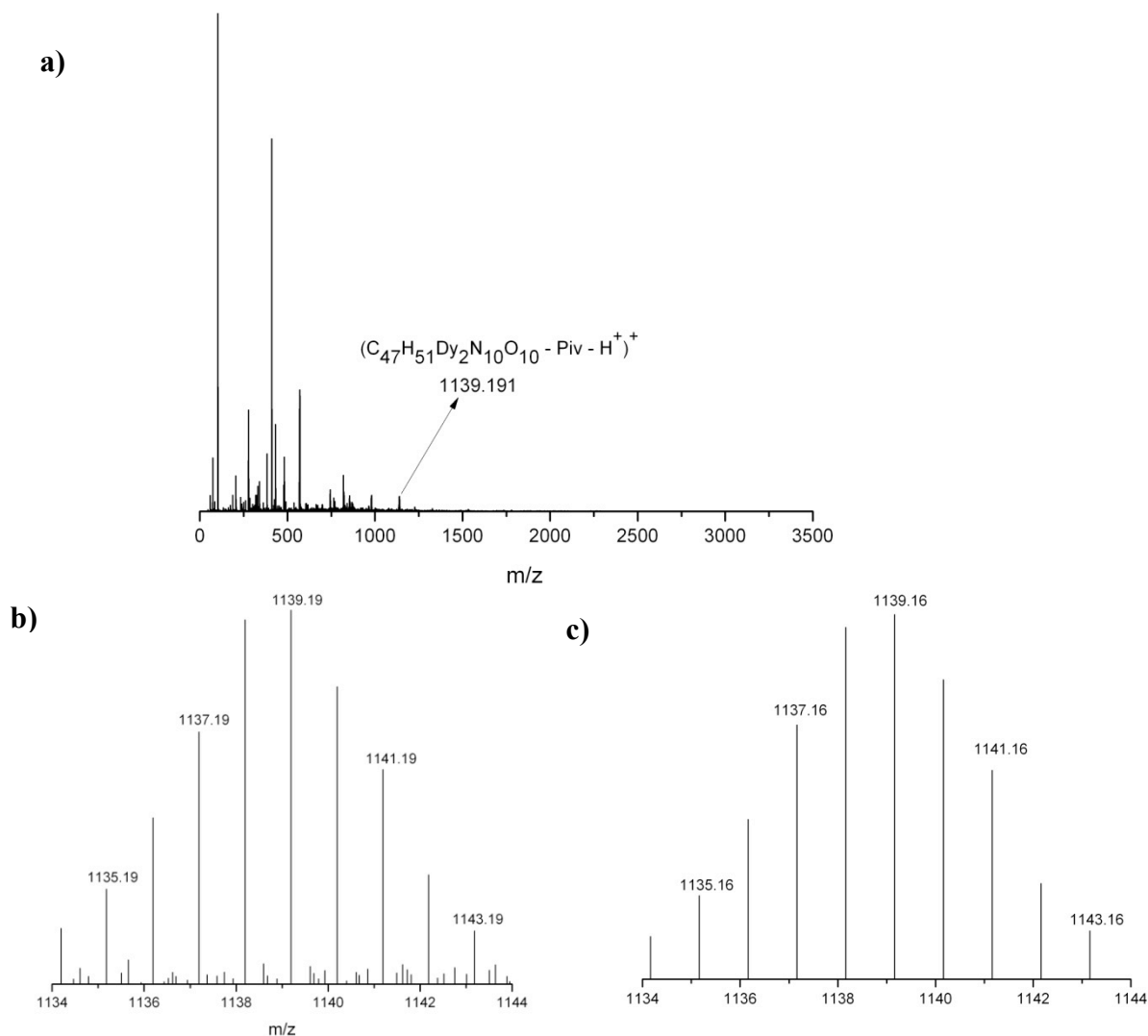


**Figure 1.** a) Full range ESI-MS spectrum of complex **1**, b) experimental and c) simulated mass spectrometry pattern of the species,  $[C_{47}H_{51}Dy_2N_{10}O_{10} - Piv - H^+]^+$ .

## X-ray Crystallography

Single-crystal X-ray diffraction data reveals that **1** comprises of a monocationic dinuclear complex,  $[\text{Dy}_2(\text{LH}_2)_2(\mu_2\text{-}\eta^1, \eta^1\text{-Piv})]^+$  and a chloride counter anion. Complex **1** crystallized in the monoclinic space group  $P2_1/c$  ( $Z = 4$ ). A perspective view of **1** is given in Figure 2 and the selected bond parameters are summarized in Table S1 (Supporting Information).

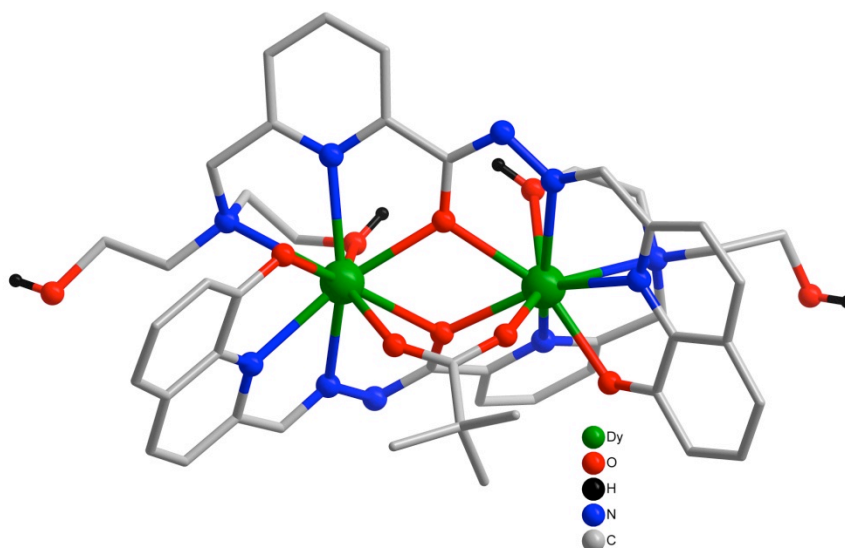


**Figure 2.** Molecular structure of the  $\{\text{Dy}_2\}$  complex in **1** (solvent molecules, selected hydrogen and chloride have been omitted for the sake of clarity).

**1** is formed by the coordination action of two doubly deprotonated ligands  $[\text{LH}_2]^{2-}$ . Within **1**, each of the two  $[\text{LH}_2]^{2-}$  bind two  $\text{Dy}^{3+}$ , simultaneously utilizing their tetradentate pockets ( $\text{O}_2\text{N}_2$ ) along with bridging enolate oxygen. While one arm of the diethanolamine of the pocket A2 binds to  $\text{Dy}^{3+}$  in a monodentate fashion, the other arm does not participate in coordination (Figure2). Apart from the binding provided by the  $[\text{LH}_2]^{2-}$ , the dinuclear framework is further strengthened

by a bridging pivalate ligand. The coordination modes of the ligands involved in the assembly of **1** are given in Figure 3.

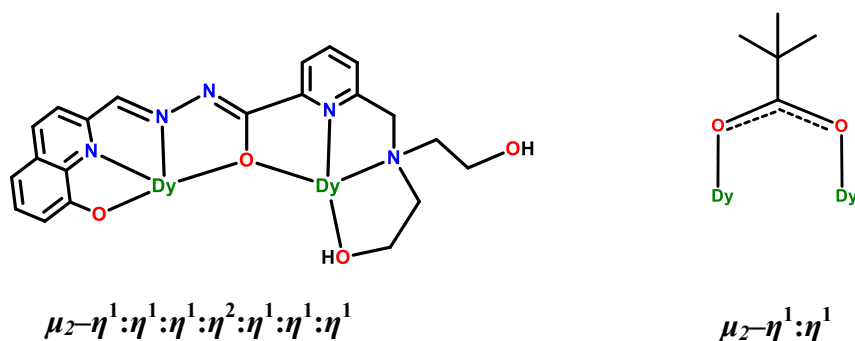


**Figure 3.** Binding modes of the  $[\text{LH}_3]^{2-}$  and pivalate ligand in **1**.

Note that in the formation of **1**, the ligand has exclusively utilized the enol form to generate the  $\text{Dy}_2\text{O}_2$  core. Both the  $\text{Dy}^{3+}$  in **1** are nine-coordinated and contain a 5O,4N coordination environment with a distorted monocapped square antiprism geometry (Figure 4).

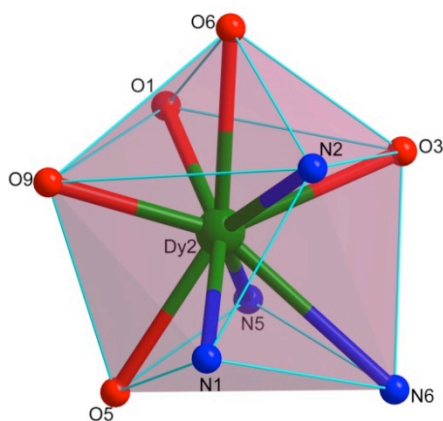


**Figure 4.** Distorted monocapped square antiprism coordination environment around  $\text{Dy}^{3+}$  in **1**.

A few comments about the metric parameters found in **1**. The Dy–N bond lengths fall in the range of 2.506–2.859(5) Å with the longest bond for Dy–N<sub>diethanolamine</sub>. The average Dy–O<sub>CH<sub>2</sub>OH</sub> bond length is 2.437(5) Å which is slightly longer than the average Dy–O<sub>hydrazone</sub> bond length,

2.408(6) Å, which in turn is longer than the average Dy–O<sub>pivalate</sub> [2.281(7) Å] and Dy–O<sub>8HQ</sub> [2.319(5) Å] bond lengths. The Dy1–O1–Dy2 [113.93(2)°] and the Dy1–O6–Dy2 [113.61(2)°] bond angles are similar and are comparable to those found in the literature.<sup>[9,10]</sup>

Complex **2** is neutral, tetranuclear and crystallized in the triclinic system (*P*-1, *Z* = 1). For **2**, the asymmetric unit contains one half of the entire molecule, *viz.*, [Dy<sub>2</sub>(LH)(OH)(Piv)<sub>2</sub>(MeOH)] (Figure 5a) and the complete molecule is generated by an inversion element which resides at the center of the molecule. A perspective view of the complex **2** is given in Figure 5b (see Table S2 for selected bond lengths and angles).

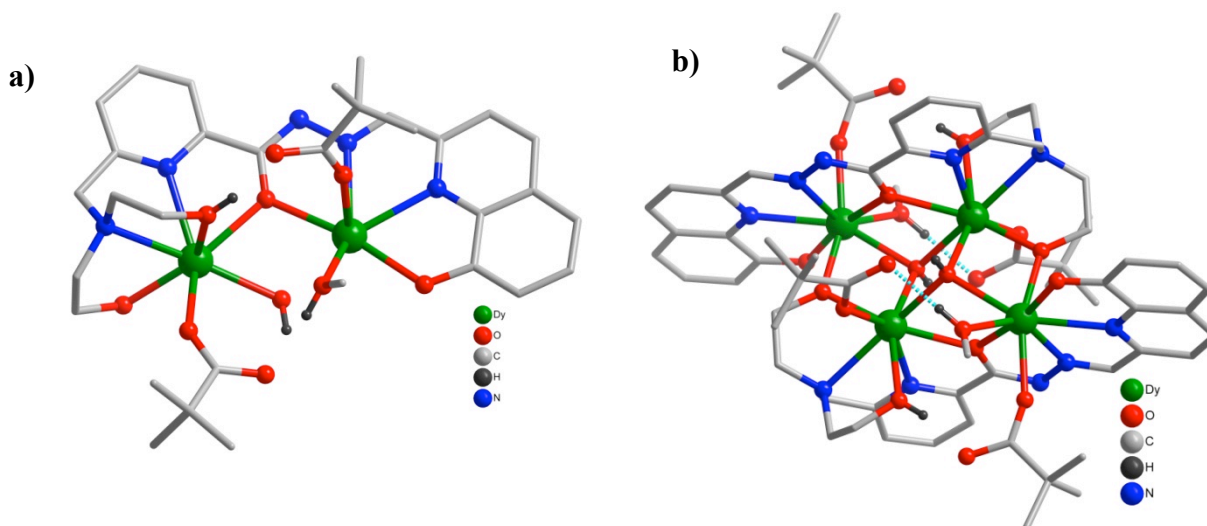


**Figure 5.** a) Asymmetric unit of **2**. b) Molecular structure of **2** (solvent molecules and selected hydrogen have been omitted for clarity).

The tetranuclear assembly in **2** is made possible by the involvement of two triply deprotonated ligands, [LH]<sup>3-</sup>, which are arranged in an almost antiparallel fashion (Figure 5). Among the nine divergent coordination sites of LH<sub>4</sub>, eight are engaged in binding with Dy<sup>3+</sup> while the other *viz.*, hydrazone N does not participate in coordination. Within **2**, each of the two ligands in their triply

deprotonated form hold two  $\text{Dy}^{3+}$  simultaneously in the two asymmetric pockets: one of them is tetradentate (P1, 2O, 2N), whereas the other one is pentadentate (3O, 2N). Both the  $\text{Dy}^{3+}$  centers within the pockets are connected to each other by a bridging hydrazine O to generate a dimeric subunit,  $[\text{Dy}_2(\text{LH})]^{3-}$  that is connected to a similar dimeric unit by a bridging ethanolamine amine, giving rise to the tetranuclear assembly (Figure 5b). In addition to the binding provided by the  $[\text{LH}]^{3-}$ , the tetranuclear assembly is further stabilized by two exogenous  $\mu_3$ -OH ligands and four monodentate pivalate ligands. Overall, each ligand has adopted a  $\mu_3$ - $\eta^1:\eta^1:\eta^1:\eta^2:\eta^1:\eta^1:\eta^1:\eta^2$  coordination mode (Figure 6), and along with the further assistance from two  $\mu_3$ -OH and four pivalate ligands the hexacationic tetranuclear core,  $[\text{Dy}_4(\text{O})_4(\text{OH})_2]^{6+}$ , is assembled, featuring a butterfly-shaped topology (Figure 7).

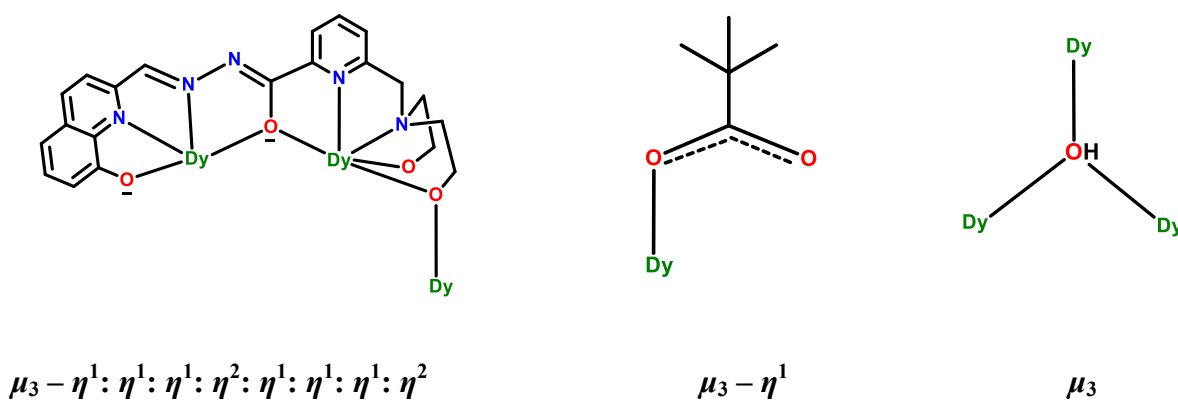


**Figure 6.** Various coordination modes of the ligands involved in the formation of **2**.

The butterfly-shaped  $\text{Dy}_4$  core is composed of four coplanar dysprosium ions: Dy1 and Dy1\* define the body while Dy2 and Dy2\* represent the two wings (Figure7). Further inspection of the  $\text{Dy}_4$  core of **2** reveals some interesting features. Considering the involvement of the two ligands, the tetranuclear core can be seen as a face-sharing lacunary dicubane structure with two missing

vertices. The central core,  $[\text{Dy}_4(\mu_3\text{-OH})_2]^{10+}$  can be divided into a pair of edge sharing isosceles triangles, whose one side is capped by  $\mu_3\text{-OH}$  (Figure 7).

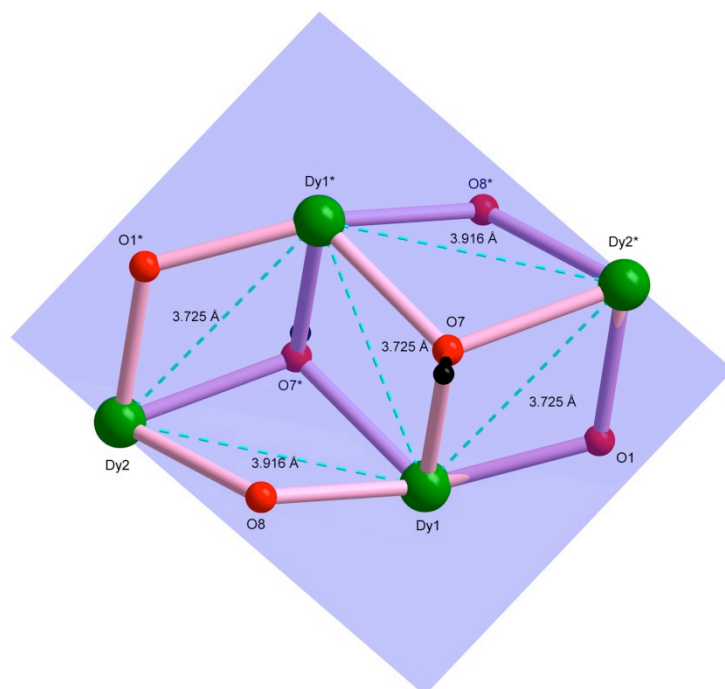


**Figure 7:** Butterfly shaped core structure in **2**.

All  $\text{Dy}^{3+}$  in **2** are eight-coordinated and can be grouped into two categories in terms of the coordination environments and geometry: Dy1 and Dy1\*, in a distorted dodecahedron geometry are surrounded by a 6O,2N environment which is provided by  $[\text{LH}]^{3-}$ , pivalate and  $\mu_3\text{-OH}$  ligands. On the other hand, Dy2 and Dy2\* possess a distorted triangular dodecahedron geometry in a 6O, 2N coordination environment with contribution from  $[\text{LH}]^{3-}$ , pivalate,  $\mu_3\text{-OH}$  and solvent MeOH (Figure 8). Metric parameters in **2**: The Dy–N bond lengths fall in the range of 2.516–2.604(5) Å, consistent with those found in the literature.<sup>[9,10]</sup> The average Dy–O bond length is 2.345(5) Å with the largest bond distance being 2.417 Å encountered in Dy–O<sub>MeOH</sub>. The

Dy–OH<sub>μ3</sub>–Dy bond angles lie in wider range (103.11–110.04(2)°) than that of the Dy–O<sub>μ2</sub>–Dy and Dy–O<sub>ethanolamine</sub>–Dy bond angles, which are almost identical, ~110.5(2)°.

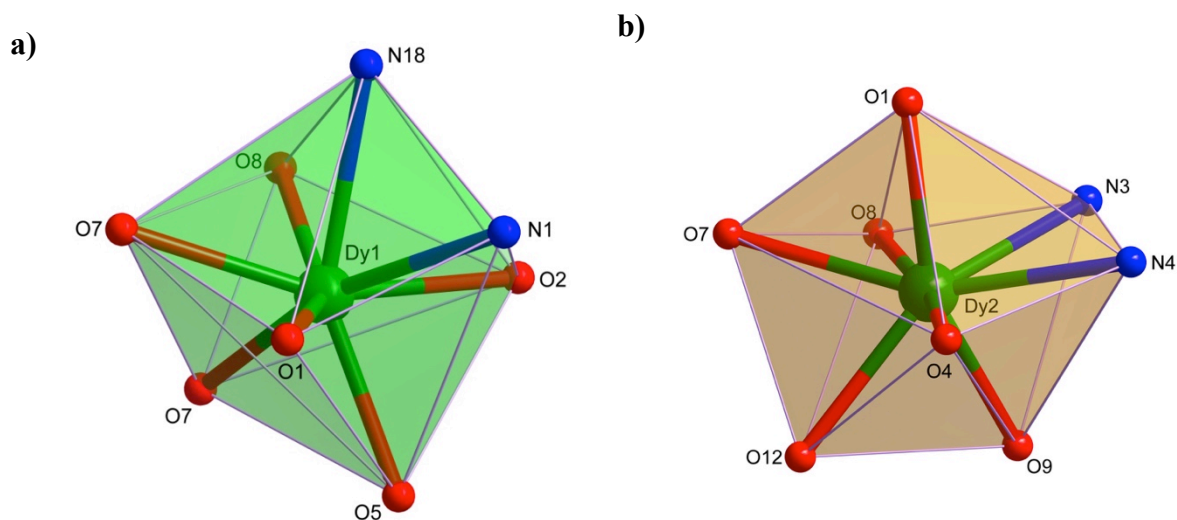


**Figure 8.** a) Distorted dodecahedron geometry around Dy1. b) distorted triangular dodecahedron geometry around Dy2 in **2**.

The molecular structure of **3** represents a homometallic hexanuclear complex with four chloride counter anions. **3** crystallized in the trigonal space group  $P\bar{3}c1$  with  $Z = 2$ . The asymmetric unit consists of one third of the entire molecular unit, namely  $[\text{Dy}_2(\text{LH}_2)(\text{tfa})(\text{OP}^t\text{Bu})(\text{Cl})]\text{Cl}_2$  (Figure 9a) and the full molecule is generated as a result of a  $C_3$  element which passes through the middle of the complex **3**. The molecular structure of **3** is given in Figure 9b and selected bond lengths and angles are summarized in Supporting Information (Figure S3).

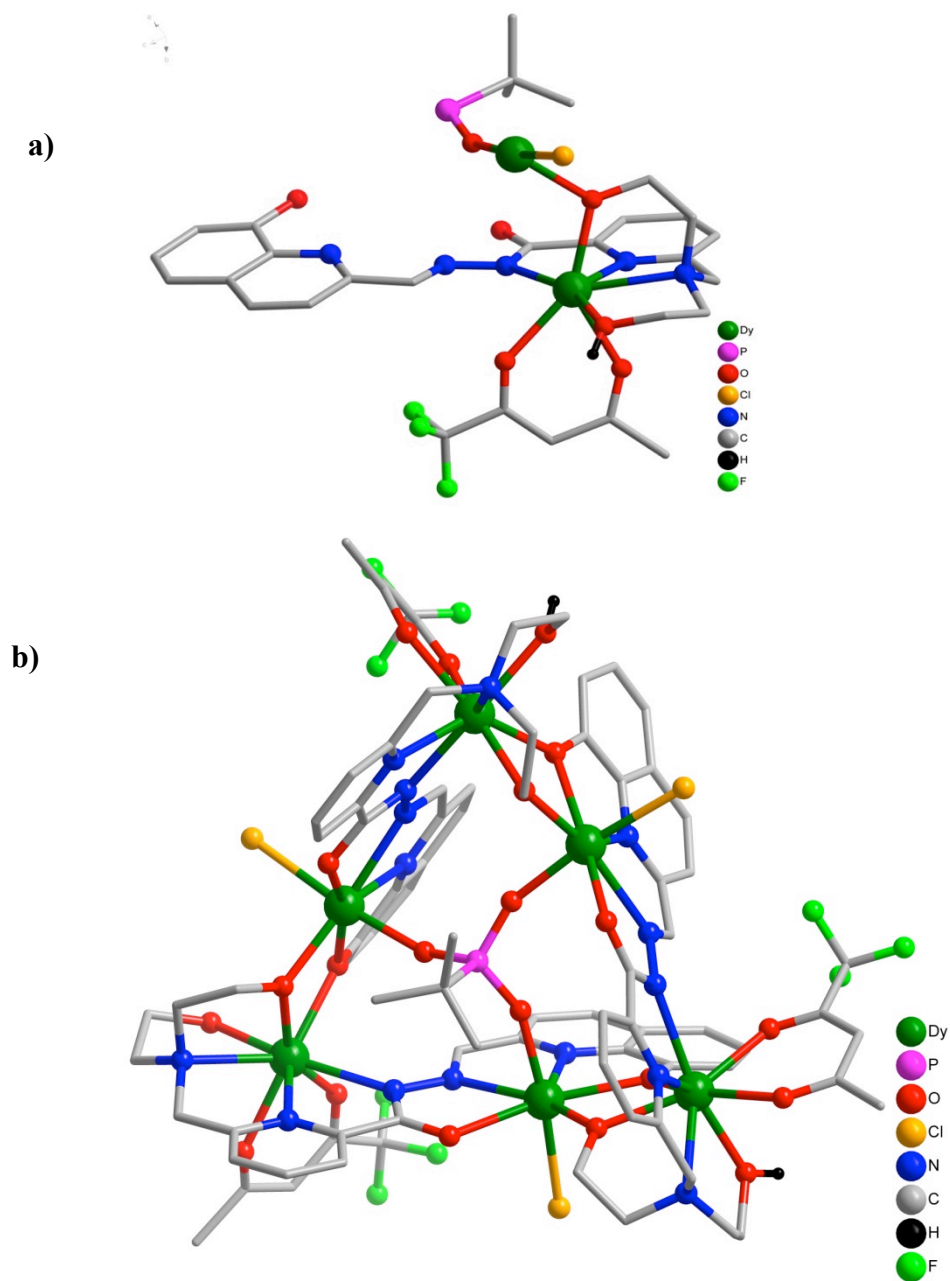


**Figure 9.** a) Asymmetric unit of **3**. b) Molecular structure of **3** (solvent molecules, selected chlorides and hydrogens have been omitted for clarity).

The formation of **3** involves three doubly deprotonated ligands,  $[\text{LH}_2]^{2-}$ , each of which are nonadentate and utilizes all the available coordinating centers. Within the complex **3**, it has been found that each ligand in a doubly deprotonated keto form accommodates two  $\text{Dy}^{3+}$  in its two asymmetric pockets [one of these is tetradentate (2O, 2N) where the other one is pentadentate (2O, 3N)] to generate a dimeric subunit  $[\text{Dy}_2(\text{LH}_2)]$  in which the two metal centers are secluded (not attached through a single-atom bridge) unlike the former two complexes, *vide supra*. The dimeric subunit thus formed is further bolstered by a chloride and *tfa* ligands: while the former is coordinated to Dy1, the latter is chelated to Dy2. Finally, three such dimeric subunits are stitched together by bridging oxygen atoms of  $[\text{LH}_2]^{2-}$  to afford a homometallic hexanuclear assembly with a topology of a perfect equilateral triangle. Apart from the binding provided by  $[\text{LH}_2]^{2-}$ , the formation of **3** is also made possible by a tertiary butyl phosphonate ligand which fits into the center of **3** by acting as a tridentate ligand to Dy1, Dy1\* and Dy1\*\*. The unique binding modes of the various ligands involved in **3** are given in Figure 10.

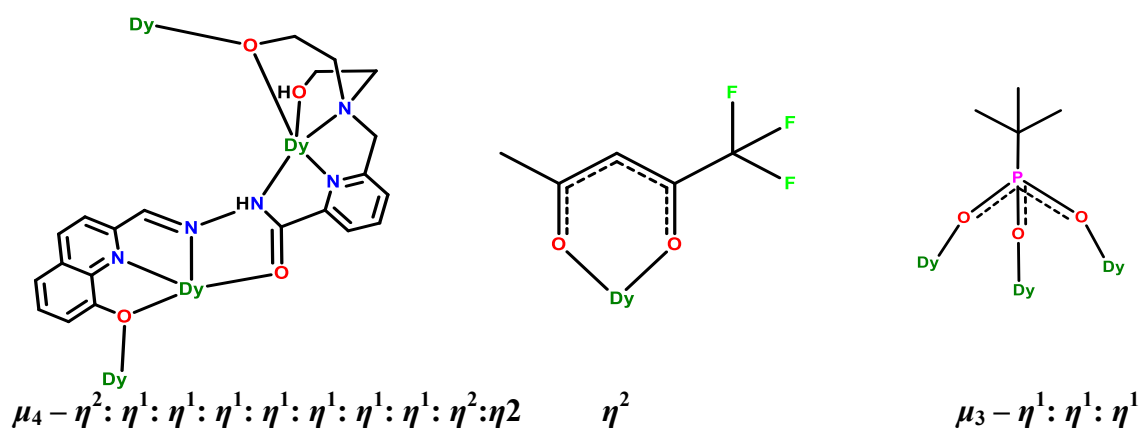


**Figure 10.** Various coordination modes of the ligands involved in the formation of **3**.

The hexanuclear core  $[\text{Dy}_6(\text{O})_6(\text{N}_2)_6(\text{O}_3\text{P}^t\text{Bu})(\text{Cl})_3]^{7+}$  comprises of six coplanar  $\text{Dy}^{3+}$  and remarkably represents a regular equilateral triangle with a side length of 9.541 Å (Figure 11a). Each side of the triangle contains three  $\text{Dy}^{3+}$  in which two metal centers being doubly bridged by O of 8-hydroxyquinoline and O of diethanolamine of  $[\text{LH}_2]^{2-}$  is segregated from the third  $\text{Dy}^{3+}$ . Interestingly, the current structural topology is quite distinct and stands unique in the homometallic hexanuclear  $\text{Dy}_6$  family.<sup>[11]</sup> Furthermore, if we exclude the ligands, the hexametallc framework can be expanded into two overlapping equilateral triangles with side lengths of 9.541 Å and 6.077 Å each (Figure 11b).

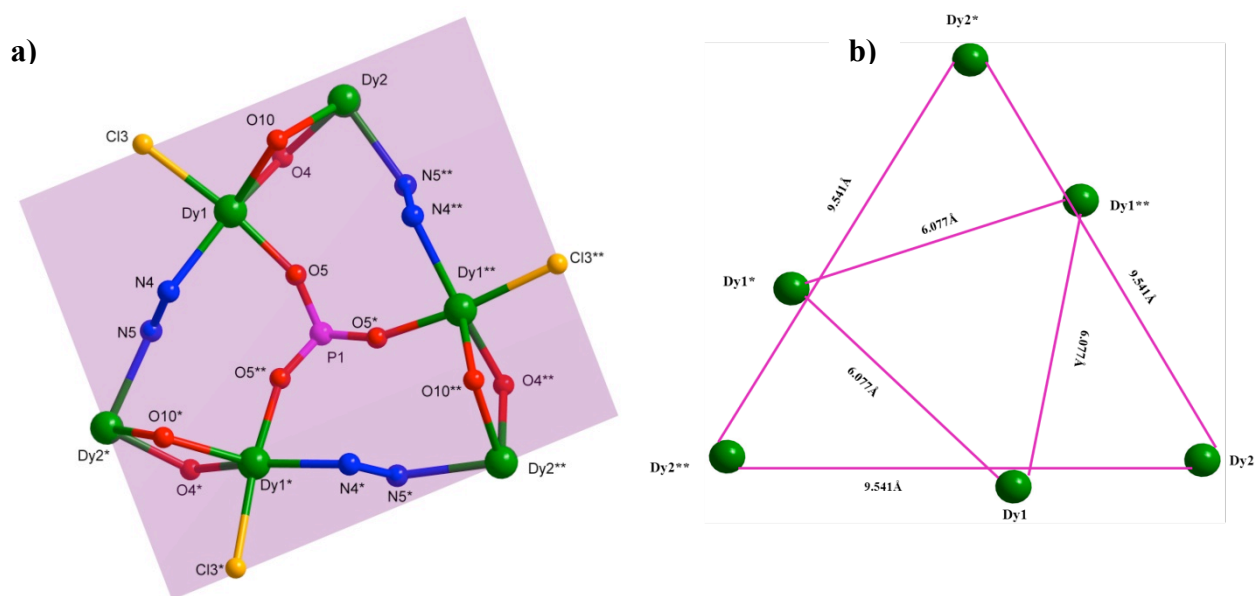


**Figure 11.** a) View of the central  $\text{Dy}_6$  core; b) Arrangement of the  $\text{Dy}_6$  unit in two overlapped equilateral triangles in **3**.

Overall, **3** comprises two crystallographically independent  $\text{Dy}^{3+}$  and can be categorized in two geometries:  $\text{Dy}_2$ ,  $\text{Dy}_2^*$  and  $\text{Dy}_2^{**}$  are eight-coordinated in a 5O,3N environment and possess a distorted square antiprism geometry (Figure 12a) while  $\text{Dy}_1$ ,  $\text{Dy}_1^*$  and  $\text{Dy}_1^{**}$  contain a 4O, 2N, Cl environment in a distorted pentagonal bi-pyramidal geometry (Figure 12b). Although known,

Dy<sup>III</sup> complexes with a pentagonal bipyramidal ligand environment are exceedingly rare<sup>[2a,b]</sup> and are unique in the hexanuclear family.<sup>[11]</sup>

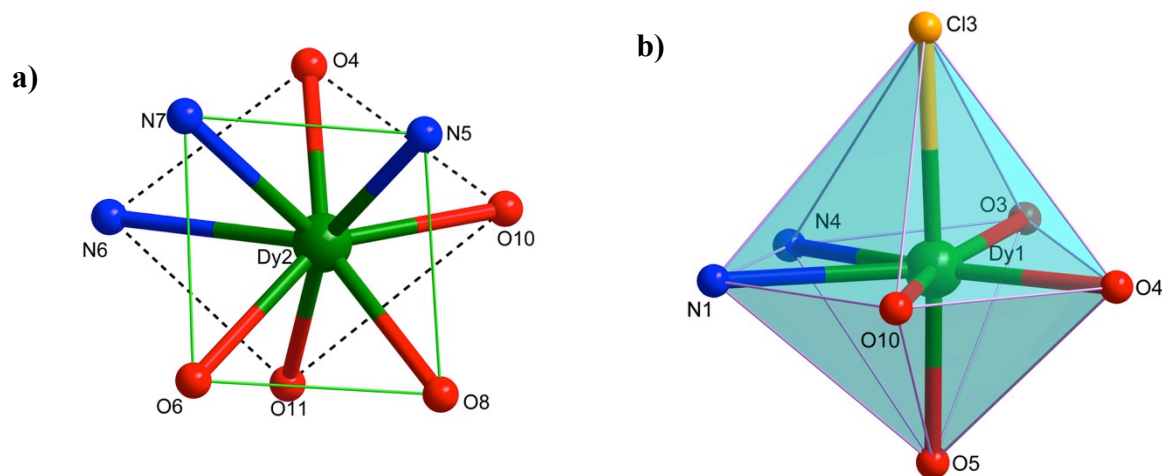


**Figure 12.** a) Distorted square antiprism geometry around Dy2; b) distorted pentagonal bipyramidal geometry around Dy1 in **3**.

The Dy–N bond lengths fall in the range of 2.490–2.591(8) Å with the largest distance for Dy–N<sub>diethanolamine</sub>. The Dy– $\mu_2$ O<sub>diethanolamine</sub> bond length is ~2.251(8) Å, which is shorter than the Dy–O<sub>diethanolamine</sub> [2.360(6)Å] but larger than Dy–O<sub>phosphonate</sub> [2.169(6)Å]. The Dy–O<sub>hydrazone</sub> and Dy–Cl bond lengths are 2.342(8) Å and 2.619(8) Å, respectively, and these values are consistent with the literature precedents.<sup>[11,9]</sup> The Dy– $\mu_2$ -O<sub>diethanolamine</sub>–Dy bond angle is 112.77(2)°, significantly larger than Dy– $\mu_2$ -O<sub>8HQ</sub>–Dy, 103.95(2)°.

Compound **4** is heptacationic and crystallized in the triclinic system in space group  $P-1$  with  $Z = 2$ . The asymmetric unit contains a full molecule *viz.*  $[\text{Dy}_{21}(\text{L})_7(\text{LH})_7(\text{tfa})_7]\text{Cl}_7$  (Figure 13) whose selected metric parameters are sorted in the Supporting Information (Table S4).

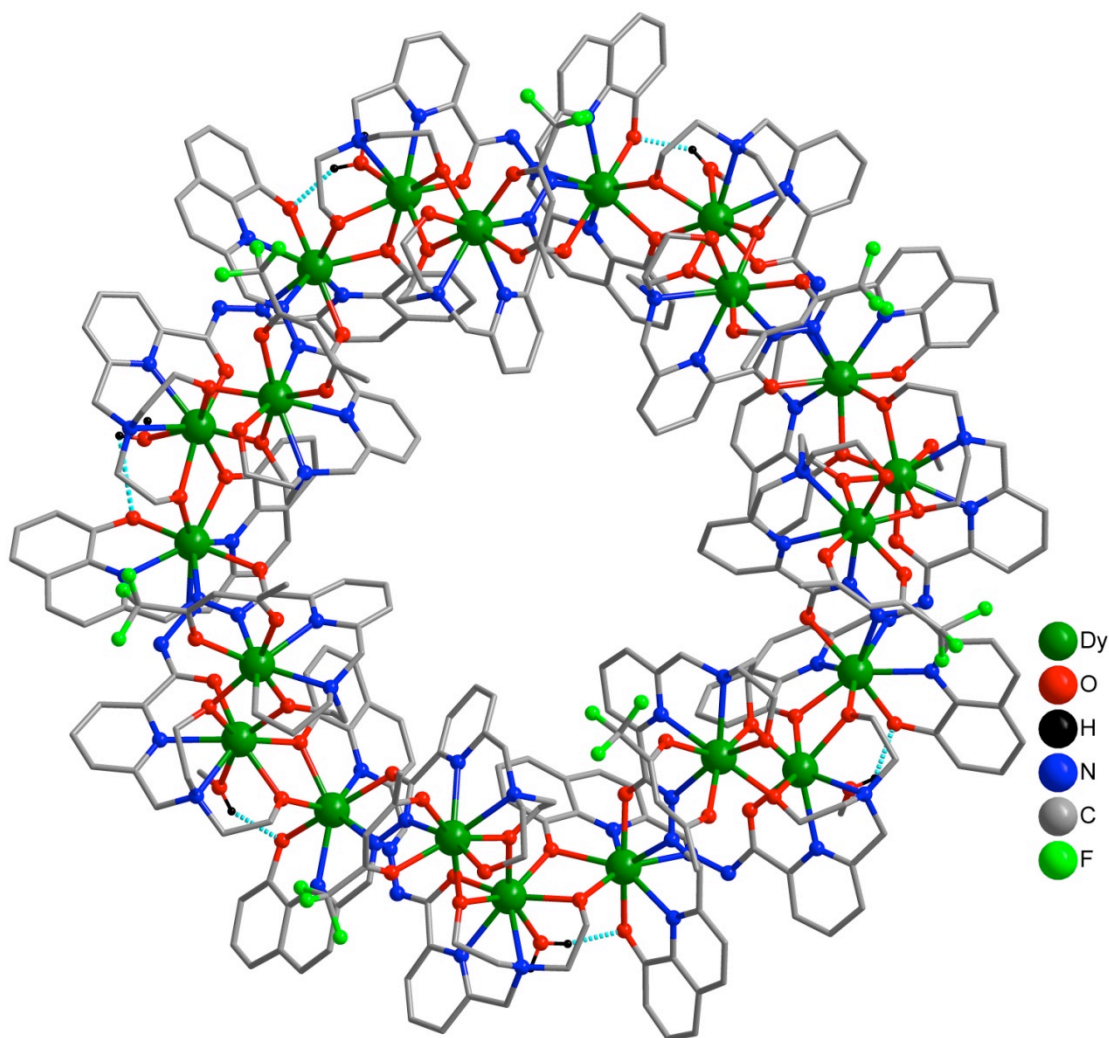


**Figure 13.** Molecular structure of **4** (solvent molecules, selected chlorides and selected hydrogens have been omitted for clarity).

**4** can be described as a single-stranded *nanowheel*, containing seven  $(\text{LH}^{3-})$ , seven  $(\text{L}^{4-})$ , and seven 1,1,1-trifluoroacetylacetonate ligands. Interestingly, both  $[\text{LH}]^{3-}$  and  $[\text{L}]^{4-}$  are present in

their enolate forms holding two  $\text{Dy}^{3+}$  in their two pockets in a segregated manner. This capability of the ligands is made possible by a  $180^\circ$  rotation across the C–C bond (displayed by  $[\text{LH}]^{3-}$ ) and a  $90^\circ$  rotation across the hydrazine N–N bond (exhibited by  $[\text{L}]^{4-}$ ) (Scheme 3). While bond rotation across the hydrazone C and benzene C is well known in the lanthanide families, hydrazine N–N bond rotation is very rare.<sup>[10b-d]</sup> The varying coordination modes of the ligands and co-ligands, as present in in **4** are shown in Figure 14.

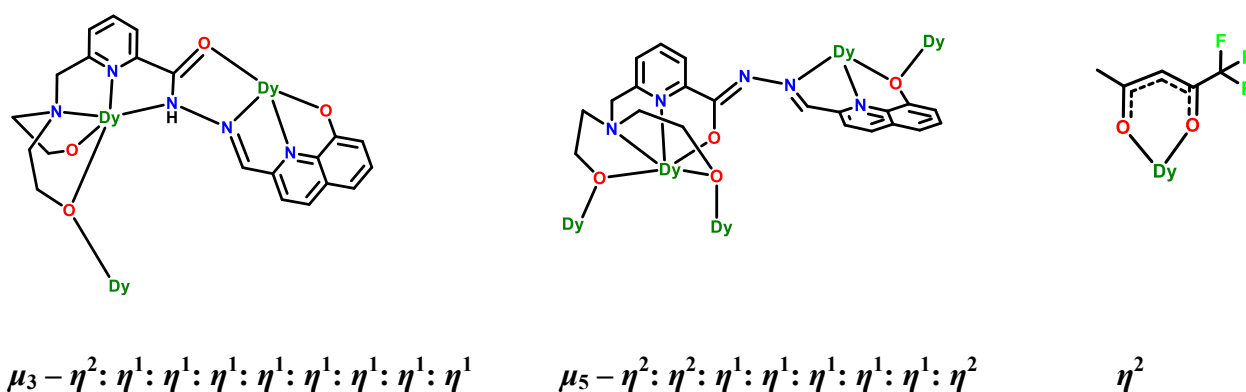


**Figure 14.** Various coordination modes of the ligands in **4**.

The formation of **4** can be understood in the following way: 1) the concerted coordination action of a  $[\text{L}]^{4-}$ ,  $[\text{LH}]^{3-}$  and 1,1,1-trifluoroacetylacetonate enables the formation of a trinuclear subunit of metallic core  $\{\text{Dy}_3\}$ ; 2) seven such subunits are doubly bridged on either side by the O of phenolate and O of the ethanolamine ligands to ultimately furnish a giant  $\text{Dy}_{21}$  nanowheel. Within the  $\text{Dy}_3$  subunit, while two adjacent  $\text{Dy}^{3+}$  are doubly bridged by the O of the ethanolamine ligands, the third  $\text{Dy}^{3+}$  stands isolated.

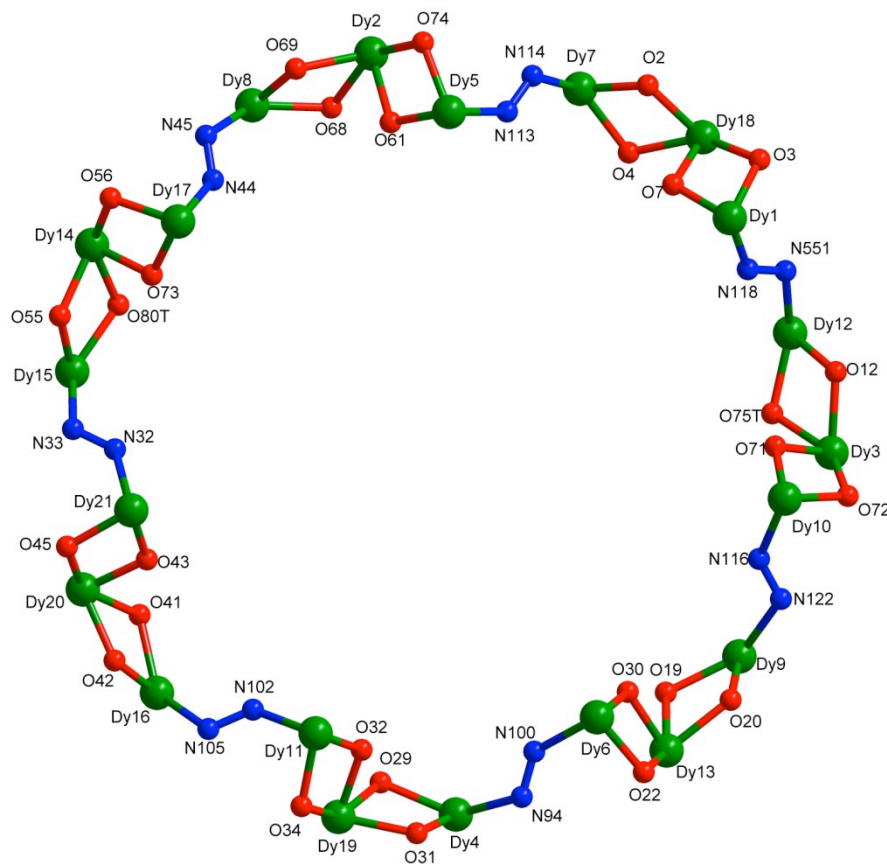


**Figure 15.** Dy<sub>21</sub> core in **4** highlighting the connection of the Dy<sub>3</sub>O<sub>4</sub> units via hydrazine nitrogen on either side.

The core of **4** comprises seven non-planar Dy<sub>3</sub>O<sub>4</sub> subunits, which in turn represent spirocycles with a Dy<sup>3+</sup> being located at each spirocyclic node (Figure 15). Within this subunit, intermetallic distances have been found to vary in a narrow range, 3.74–3.81(6) Å, whereas Dy–O–Dy bond angles lie in a much wider range, 108.2–113.69(2)°. Remarkably, seven such units are interlinked via hydrazine nitrogen atoms to furnish a 45-membered non-planar macrocycle when considering the shortest Dy–O–Dy pathways (Figure 15). Apart from these features, the space-filling model of **4** reveals that the internal diameter, external diameter and the width are 0.96 nm, 3.3 nm and 1.2 nm respectively, suggesting that this nanowheel falls in the smallest nanoparticle

domain (Figure 16). It is of interest to mention that high-nuclear lanthanide complexes that are SMMs are still quite sparse: previously  $\text{Dy}_{22}$ ,  $\text{Dy}_{24}$ ,  $\text{Dy}_{26}$ ,  $\text{Dy}_{27}$ ,  $\text{Dy}_{28}$  and  $\text{Dy}_{30}$  complexes have been reported, which were prepared using an anion-template synthesis.<sup>[12]</sup> Moreover, single-stranded high nuclear lanthanide nanowheels are very rare with an example containing  $\text{Gd}_{18}$  being the largest known so far.<sup>[13]</sup> The present  $\text{Dy}_{21}$  complex is one of a kind; it is devoid of oxide/hydroxide ligands and is also prepared from a non-template synthetic strategy unlike the previous instances.<sup>[12]</sup>

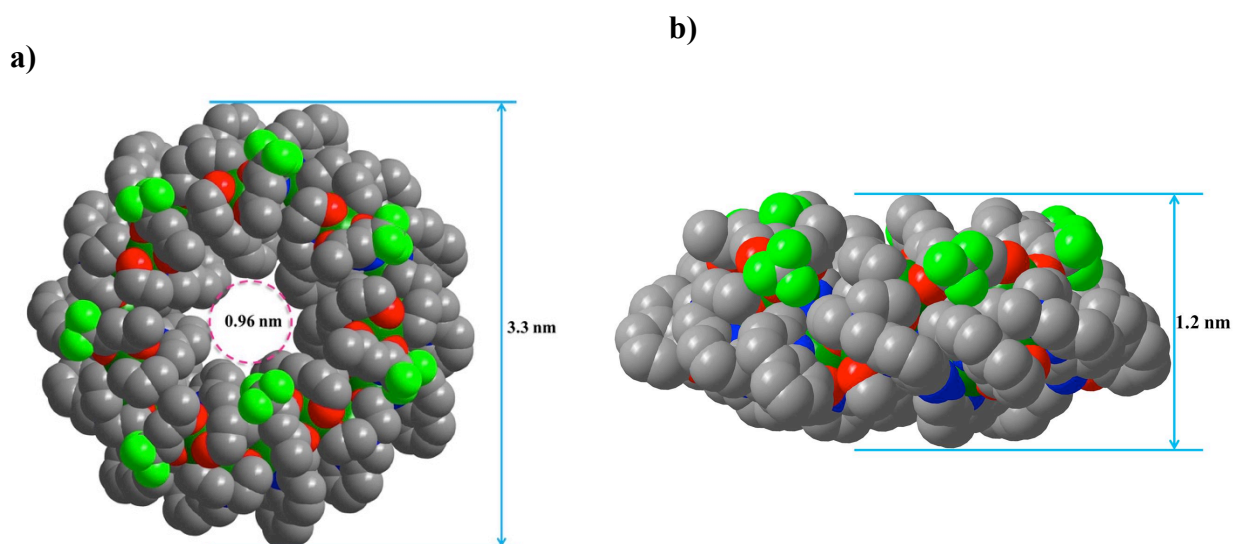


**Figure 16.** Space filling model of **4**. The inner and outer diameters (a) and the width (b) of the nanowheel are shown.

**4** consists of three crystallographically independent lanthanide centers which can be grouped into two categories depending on their geometry: 1) distorted triangular dodecahedron (4N,4O) (Figure 17a) and 2) distorted square-antiprism geometry (2N,6O) (Figure 17b) 3N, 5O (Figure 17c).

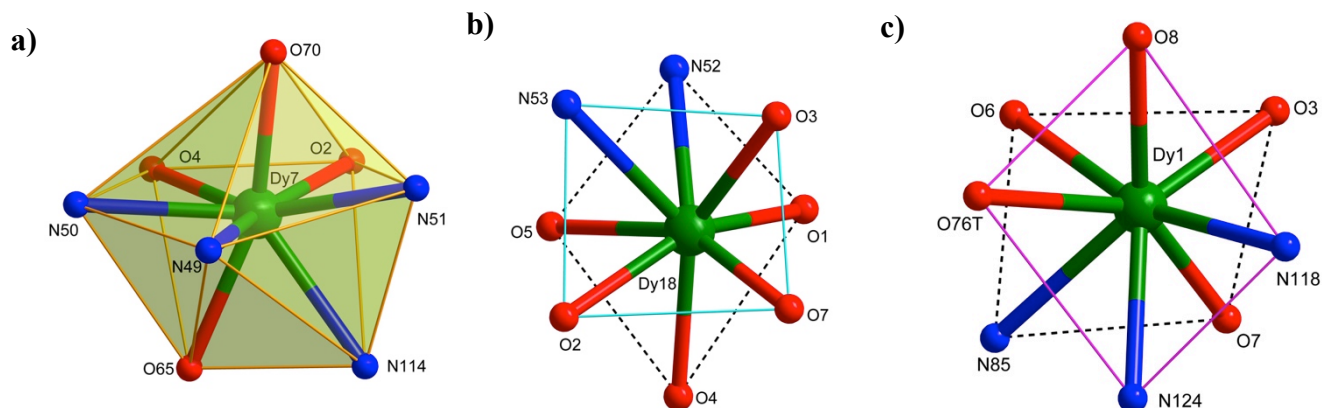


**Figure 17.** The Dy<sup>3+</sup> coordination environments in **4**: a) the distorted triangular dodecahedron 4N,4O environment; b) the distorted square anti-prism 2N,6O environment; c) the distorted square anti-prism 3N,5O environment.

Several intramolecular and intermolecular interactions are persistent in complexes **1–4**, and some of these led to remarkable supramolecular motifs that are described in the Supporting Information (Figures S3, S4).

In spite of the variation of nuclearity and local differences in the coordination modes of the various ligands, the metric parameters found in complexes **1–4** are grossly similar as summarized in Table 1, indicating the flexible nature of the ligands that can accommodate the formation of complexes with varying nuclearities without causing undue steric strain.

**Table 1:** Comparison of bond distances (Å) and angles (°) in **1**, **2**, **3** and **4**.

Parameters	<b>1</b>	<b>2</b>	<b>3</b>	<b>4</b>
Dy–O <sub>8HQ</sub>	2.319(4)	2.323(5)	2.379(6)	2.357(7)

Dy–O <sub>hydrazone</sub>	2.408(5)	2.384(5)	2.342(6)	2.324(7)
Dy–O <sub>diethanolamine</sub>	2.437(4)	2.393(5)	2.360(6)	2.334(7)
Dy–N <sub>py</sub>	2.553(6)	2.529(6)	2.490(8)	2.479(5)
Dy–N <sub>diethanolamine</sub>	2.849(6)	2.604(6)	2.591(8)	2.589(5)
Dy–O <sub>hydrazone</sub> –Dy	113.77(2)	110.45(2)		
Dy–O <sub>diethanolamine</sub> –Dy		110.62(2)	112.77(2)	113.06(2)

### Magnetic studies

Results of ac and dc susceptibility measurements of **1** are shown in Figure 18. The dc data are represented by  $\chi_m T$  vs.  $T$  and  $M_m$  vs.  $B$  plots. At 290 K,  $\chi_m T$  is  $28.06 \text{ cm}^3 \text{ K mol}^{-1}$ , *i.e.* close to the upper limit of the range  $26.02\text{--}28.10 \text{ cm}^3 \text{ K mol}^{-1}$  expected<sup>14</sup> for two non-interacting Dy<sup>3+</sup> centers. Upon lowering the temperature,  $\chi_m T$  is almost constant down to 50 K ( $27.62 \text{ cm}^3 \text{ K mol}^{-1}$ ), decreases to a minimum at 6.5 K ( $26.06 \text{ cm}^3 \text{ K mol}^{-1}$ ) and increases to  $26.38 \text{ cm}^3 \text{ K mol}^{-1}$  at 2.0 K. Since the decrease of the  $\chi_m T$  values is small, the exchange interaction between both Dy<sup>3+</sup> centers is potentially weak, and presumably of ferromagnetic nature since the thermal depopulation of the  $m_J$  sublevels (that are split into Kramers' doublets due to the ligand field) usually causes a sharper decline of  $\chi_m T$ . The observation of the minimum at low temperatures may hint at intermolecular interactions such as packing effects. The molar magnetization  $M_m$  as a function of the applied field  $B$  is linear up to approximately 0.5 T, and reaches  $11.0 N_A \mu_B$  at 5 T. Although the magnetization hints at saturation for  $B > 2$  T, the small but distinct slope of the  $M_m$  vs.  $B$  data shows that the compound is not saturated at 5 T, and the saturation magnetization is

thus potentially larger as well known for lanthanide centers.<sup>14</sup> Since  $11.0 N_A \mu_B$  is above the saturation magnetization of a single free  $\text{Dy}^{3+}$  ion ( $g_J J N_A \mu_B = 10 N_A \mu_B$ ), the exchange interactions are weak, and may be antiferromagnetic or ferromagnetic.

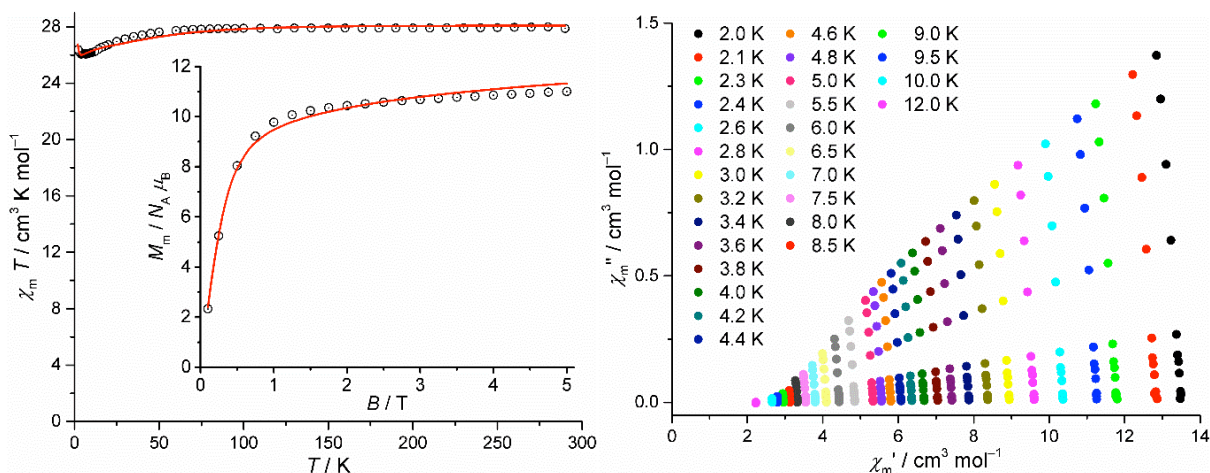


**Figure 18.** Left: temperature dependence of  $\chi_m T$  of **1** at 0.1 Tesla; inset: molar magnetization  $M_m$  vs. applied field  $B$  at 2.0 K: experimental data (open circles), least-squares fit (solid lines). Right: Cole-Cole plot of in-phase  $\chi_m'$  vs. out-of-phase  $\chi_m''$  ac magnetic susceptibility data at zero bias field.

In a tentative approach, the dc data were modeled employing the “full” model Hamiltonian using the computational framework CONDON.<sup>15</sup> The primary challenge in such an approximate model concerns the treatment of the  $\text{Dy}^{3+}$  ligand fields, where in compound **1** the 5O,4N coordination geometries are very similar but strictly speaking without any symmetry elements (Figure 4). This would mean that a total of 27 ligand field parameters per  $\text{Dy}^{3+}$  site would be needed, inevitably resulting in over-parameterization in lieu of additional experimental data on the magnetic states (e.g. derived from inelastic neutron scattering, electron absorption spectroscopy etc.). As such, we are forced to approximate the actual  $C_1$ -symmetric ligand fields by a higher-symmetry ligand field for both  $\text{DyO}_5\text{N}_4$  environments. The rationale behind this approximation is that the number

of independent and non-zero ligand field parameters is drastically reduced from 27 if higher-symmetry elements are present; moreover, small geometric deviations from an ideal geometry of a given point group are known to result only in marginal or small changes in the (otherwise vanishing) parameters.

The site symmetry approximation is derived from continuous shape measures (CShM; derived via SHAPE<sup>16</sup>) that are weighed against the symmetry-related number of non-vanishing ligand field parameters. There are two approximate geometries describing the structure of the two Dy<sup>3+</sup> environments in **1**: capped square antiprism ( $C_{4v}$ ) and tri-capped trigonal prism ( $D_{3h}$ ). The best match of these two are spherical capped square antiprisms with CShM of 3.318 and 3.063, followed by spherical tri-capped trigonal prisms with moderately worse CShM (3.788 and 3.868), tri-capped trigonal prisms (4.095, 4.352), and capped square antiprisms (4.149, 4.332). By comparison of the magnitudes of the CShM, the smallest differences of CShM of both sites and the number of non-zero ligand field parameters ( $C_{4v}$ : 5,  $D_{3h}$ : 4), we arrive at the  $D_{3h}$  approximation as the best compromise for **1**. To emphasize the exploratory nature of this approach, we have detailed the least-squares fitting (that otherwise employs standard parameters for discrete Dy<sup>3+</sup> ions<sup>17</sup>) in the Supporting Information. The key results from the least-squares fit, which reproduces the temperature-dependent low-field susceptibility and the field-dependent low-temperature magnetization data of **1** relatively well (Figure 18), are the following:  $J$  is positive ( $+0.25\pm 0.04\text{ cm}^{-1}$ ) and therefore represents a ferromagnetic exchange interaction of medium strength regarding lanthanide–lanthanide interactions. Intermolecular interactions are close to negligible. The total ligand field splitting of the ground state ( ${}^6\text{H}_{15/2}$ ) with its  $2J+1$  substates amounts to *ca.*  $170\text{ cm}^{-1}$  with the first excited substate at  $9.7\text{ cm}^{-1}$  above the ground state.

The magnetic ac susceptibility data are shown in Figure 18 as Cole-Cole plot and reveal slow relaxation at zero bias field for  $T \leq 10$  K. However, the curvatures of the  $\chi_m''$  vs.  $\chi_m'$  data for each temperature are too small for fitting a generalized Debye expression.<sup>18</sup> To enhance the curvatures, frequencies significantly exceeding what is possible with our available experimental setup would have to be applied. It should be noted that the mixture of wavefunctions in the ground state (60%  $m_J = \pm 5/2$ , 40%  $m_J = \pm 7/2$  states according to the tentative model fit) that favors the fast QTM relaxation process, as well as the small energy gap between the ground and first excited states, could explain why no maxima are observed in the  $\chi_m''$  vs.  $\chi_m'$  plots above 2 K for compound **1**.

Solely dc susceptibility data of **2** are shown in Figure 19, since the ac data did not reveal any out-of-phase component. The  $\chi_m T$  vs.  $T$  data show a value of  $52.97 \text{ cm}^3 \text{ K mol}^{-1}$  at 290 K. This value lies within the range  $52.04\text{--}56.20 \text{ cm}^3 \text{ K mol}^{-1}$  expected<sup>14</sup> for four non-interacting  $\text{Dy}^{3+}$  centers. Upon cooling compound **2**,  $\chi_m T$  continuously increases to a maximum of  $55.50 \text{ cm}^3 \text{ K mol}^{-1}$  at 40 K, subsequently decreases to a minimum of  $53.18 \text{ cm}^3 \text{ K mol}^{-1}$  at 4.0 K, and finally increases to  $53.90 \text{ cm}^3 \text{ K mol}^{-1}$  at 2.0 K. The observation of both maximum and minimum of the detected magnitude reveals the presence of both weak antiferromagnetic as well as ferromagnetic exchange interactions in **2**. In addition to intramolecular exchange interactions, the minimum at low temperatures may hint at intermolecular interactions. The molar magnetization  $M_m$  is a linear function of  $B$  up to approximately 0.5 T, and reaches  $22.7 N_A \mu_B$  at 5 T. As for **2**,  $M_m$  hints at saturation for  $B > 2$  T, but a small and distinct slope of the  $M_m$  vs.  $B$  data is observed, and the saturation magnetization is thus potentially larger. Due to the value of  $22.7 N_A \mu_B$  at 5 T, the

exchange interactions may be antiferromagnetic and/or ferromagnetic. An exploratory approach to model the magnetic dc data of **2** is given in the Supporting Information.

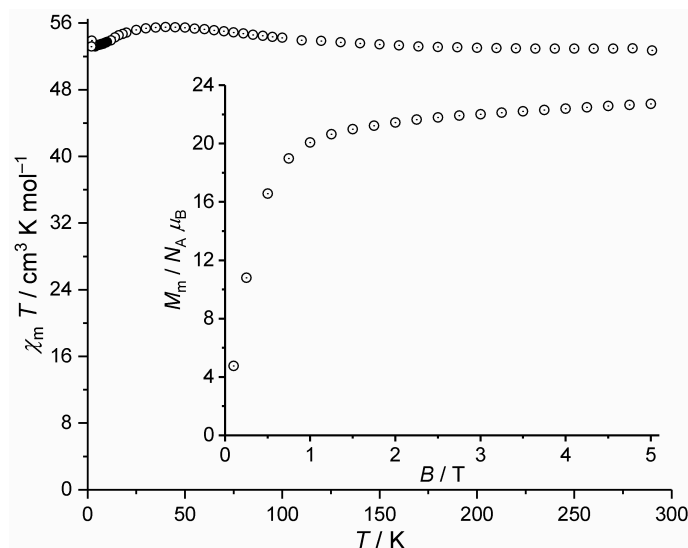


**Figure 19.** Temperature dependence of  $\chi_m T$  of **2** at 0.1 Tesla; inset: molar magnetization  $M_m$  vs. applied field  $B$  at 2.0 K.

The dc data of **3** are shown in Figure 20, and the ac data in Figure 21. At 290 K, the  $\chi_m T$  data reaches a value of  $83.41 \text{ cm}^3 \text{ K mol}^{-1}$ , which lies in the range  $78.06\text{--}84.30 \text{ cm}^3 \text{ K mol}^{-1}$  expected<sup>14</sup> for six non-interacting  $\text{Dy}^{3+}$  centers. With decreasing  $T$ ,  $\chi_m T$  continuously decreases down to  $67.03 \text{ cm}^3 \text{ K mol}^{-1}$  at 2.0 K. This is potentially due to the thermal depopulation of the  $m_j$  sublevels while weak antiferromagnetic exchange interactions may also be partly causing this dependence of  $\chi_m T$  on temperature. A slight change of the slope at approximately 7 K indicates either small paramagnetic impurities or very weak intra- or intermolecular exchange interactions.  $M_m$  vs.  $B$  is linear up to approximately 0.5 T, reaching  $31.4 N_A \mu_B$  at 5 T. As for **1** and **2**,  $M_m$  hint at saturation for  $B > 2$  T, but a small and distinct slope of the  $M_m$  vs.  $B$  data is observed, and the saturation magnetization is thus potentially larger. Due to the value of  $31.4 N_A \mu_B$  at 5 T, the exchange interactions may be antiferromagnetic and/or ferromagnetic.

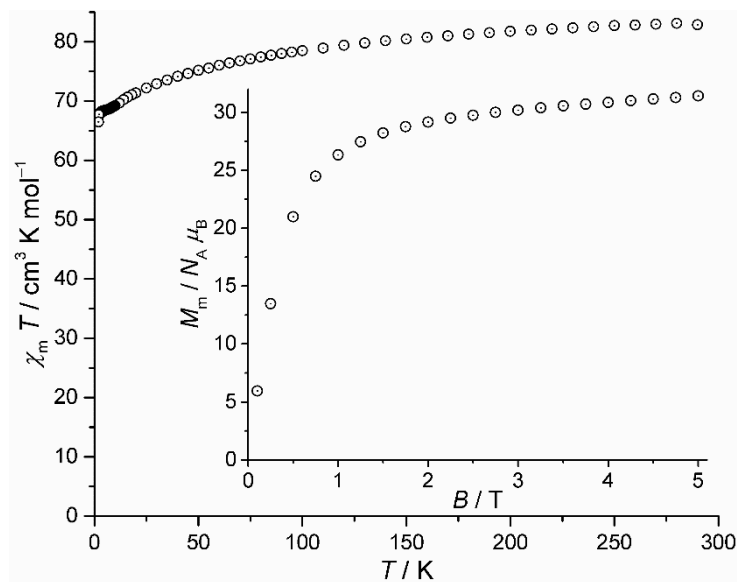


**Figure 20.** Temperature dependence of  $\chi_m T$  of **3** at 0.1 Tesla; inset: molar magnetization  $M_m$  vs. applied field  $B$  at 2.0 K.

The magnetic ac susceptibility data are shown in Figure 21 as Cole-Cole plot and reveal slow relaxation at zero bias field for  $T \leq 20$  K. However, the curvatures of the  $\chi_m''$  vs.  $\chi_m'$  data for each temperature are quite small since a maximum is not observed in the  $\chi_m''$  vs. frequency ( $f$ ) data within the limits of our experimental setup. A generalized Debye expression<sup>18</sup> has been fitted to the data (least-squares fits are shown as solid lines in the Cole-Cole plot), and the obtained magnetic relaxation times  $\tau$  are plotted against  $T^{-1}$  in a semi-logarithmical representation. The distribution of relaxation times  $\alpha = 0.17 \pm 0.02$  suggests the existence of few relaxation pathways. To determine the characteristic attempt time  $\tau_0$  and effective energy barrier  $U_{\text{eff}}$ , the expression  $\tau = \tau_0 \cdot \exp[U_{\text{eff}}/(k_B T)]$  (Boltzmann constant  $k_B$ ) is fitted to the data for  $T \geq 4.0$  K. The least-squares fit yields  $\tau_0 = (2.6 \pm 0.2) \times 10^{-5}$  s,  $U_{\text{eff}} = (2.8 \pm 0.3) \text{ cm}^{-1}$  representing a small effective energy barrier.<sup>19</sup> The attempt time  $\tau_0$  is rather large to account for an Orbach relaxation process although similar or larger values have been reported for SMMs comprising multiple lanthanides.<sup>19</sup> Fitting

a Raman or quantum tunneling relaxation equation to the data did, however, not yield a meaningful (and thus potentially better) result. We thus cannot exactly identify the precise nature of the observed relaxation process.

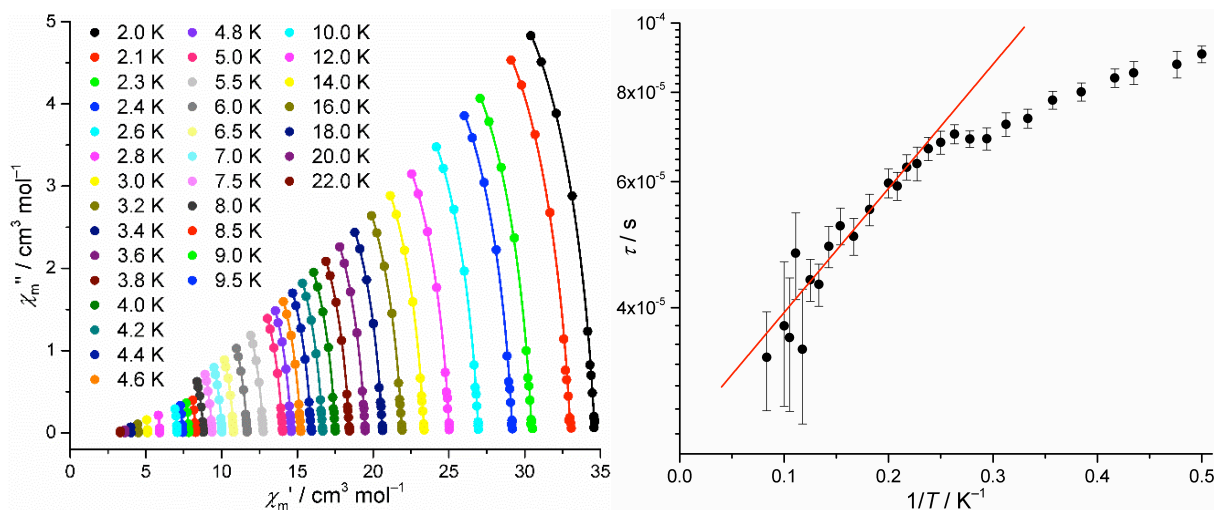


**Figure 21.** Left: Cole-Cole plot of in-phase  $\chi_m'$  vs. out-of-phase  $\chi_m''$  ac magnetic susceptibility data of **3** at zero bias field. Right: relaxation time  $\tau$  vs.  $T^{-1}$ ; experimental data (full circles), least-squares fits (left: to generalized Debye expression, right: to Arrhenius expression) (solid lines).

The temperature dependence of  $\chi_m T$  for complex **4** ( $\chi_m$  is the molar magnetic susceptibility per  $\text{Dy}_{21}$  unit) under an applied magnetic field of 0.1 T in the temperature range 300–2 K is given in Figure 22. The room temperature  $\chi_m T$  value for **4** of  $295.6 \text{ cm}^3 \text{ mol}^{-1} \text{ K}$  is close to that expected for 21 non-interacting  $\text{Dy}^{3+}$  ions of  $297.78 \text{ cm}^3 \text{ mol}^{-1} \text{ K}$  ( $4f^9$ ,  $J=15/2$ ,  $g_J=4/3$ ,  ${}^6H_{15/2}$ ) in the free-ion approximation. On lowering the temperature, the  $\chi_m T$  steadily decreases down to  $\sim 25 \text{ K}$  and finally drops off abruptly to reach a value of  $192.2 \text{ cm}^3 \text{ K mol}^{-1}$  at 2 K. This behavior is due to the thermal depopulation of the  $m_J$  sublevels of the  ${}^{2S+1}\Gamma_J$  ground state of the  $\text{Dy}^{3+}$  ion, which are originated by the crystal field, together with weak  $\text{Ln}^{3+}\cdots\text{Ln}^{3+}$  antiferromagnetic interactions.

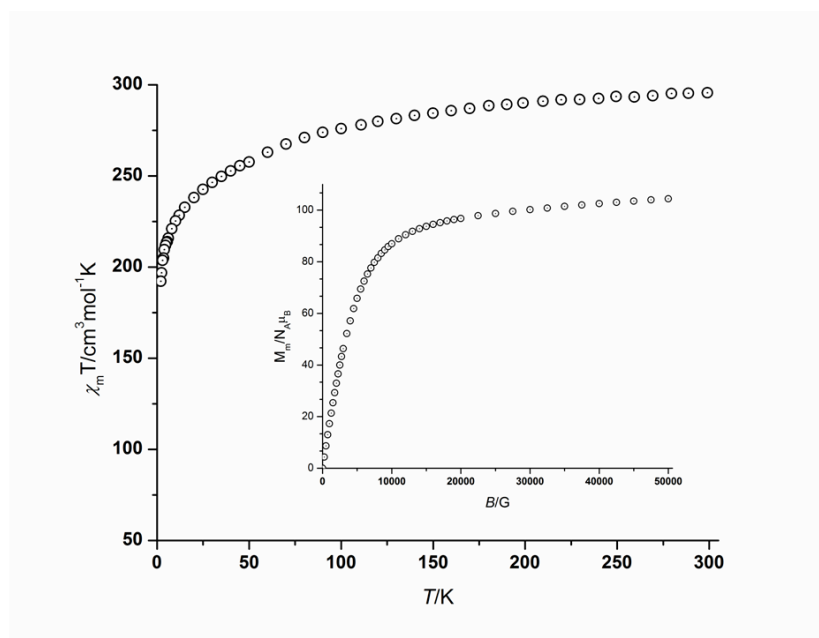


**Figure 22.** Temperature dependence of the  $\chi_m T$  for compound **4**. Field dependence of the magnetization (inset).

The field dependence of the magnetization at 2 K (Figure 22 inset) shows a rapid increase of the magnetization up to 2 T and then a linear increase at high field to reach values of  $109.9 N_A \mu_B$ , which is significantly smaller than the expected saturation magnetization value,  $M_S / N_A \mu_B = 21 g_J J = 210$ , for twenty-one  $\text{Dy}^{3+}$  ions. This low value suggests the presence of a significant magnetic anisotropy arising from the ligand-field effects. In fact, the observed values at 5 T per  $\text{Ln}^{3+}$  ion are similar those estimated for mononuclear  $\text{Ln}^{3+}$  complexes where the ligand-field effects have been considered.<sup>20</sup>

Dynamic ac magnetic susceptibility measurements as a function of the temperature at different frequencies on a microcrystalline powder sample of **4** show frequency-dependent in-phase ( $\chi'$ ) and out-of-phase ( $\chi''$ ) signals below 15 K at zero field but without exhibiting any maximum above 2 K at frequencies reaching 1400 Hz. This could indicate SMM characteristics with either a thermal

energy barrier for the reversal of the magnetization that is not high enough to block the magnetization in one of the equivalent orientations (parallel or antiparallel to the polarizing field) above 2 K or there exists quantum tunneling of the magnetization (QTM), leading to a reversal magnetization rate that is too fast to observe the maximum in the  $\chi_m''$  above 2 K. Ac measurements studies in the presence of a small external dc field of 1000 Oe were performed to try to fully or partly suppress the quantum tunneling relaxation of the magnetization (this field was chosen because it induces the slowest relaxation of the magnetization). The results (Figure 23) show that the  $\chi_m''$  signals appear virtually in the same temperature range and exhibit similar intensity as for the measurements under zero dc applied field. However, broad shoulders can be observed in the 10–4 K temperature range for frequencies above 800 Hz with a tail that increases in intensity as the temperature is lowered below 4 K. This fact reveals that the quantum tunneling of magnetization has not been efficiently suppressed, which could be due to the existence of intermolecular magnetic dipolar interactions and/or electronuclear hyperfine interactions. The broadness of the shoulders observed above 800 Hz could be due to the existence of three nearly crystallographically independent  $\text{Dy}^{3+}$  in the structure which could exhibit different relaxation processes with different energy barriers for the flipping of the magnetization. An appropriate manner to try to eliminate the intermolecular interactions and therefore the QTM process would be that of diluting the sample by co-crystallization with an isostructural diamagnetic complex, such as  $\text{Y}^{\text{III}}_{21}$ . However, all attempts to obtain the isostructural  $\text{Dy}^{3+}/\text{Y}^{3+}$  magnetic diluted complex were unsuccessful. As in this case the relaxation times cannot be extracted from the fitting to the Debye model of the frequency and temperature dependence of the  $\chi_m''$  signals, the energy barrier has been crudely estimated with the following equation assuming that only one relaxation process occurs:

$$\ln(\chi''/\chi') = \ln(\omega\tau_0) + U_{\text{eff}}/k_{\text{B}}T$$

The fitting of the experimental  $\chi''/\chi'$  data to eq. 1 (Figure 22 inset), leads to the following parameters:  $U_{\text{eff}} \approx 8.0 \text{ cm}^{-1}$  and  $\tau_0 \approx 3 \times 10^{-6} \text{ s}$ . The extracted  $\tau_0$  value is in the range usually found for lanthanide containing SMMs ( $10^{-6} - 10^{-12} \text{ s}$ ).<sup>19</sup>

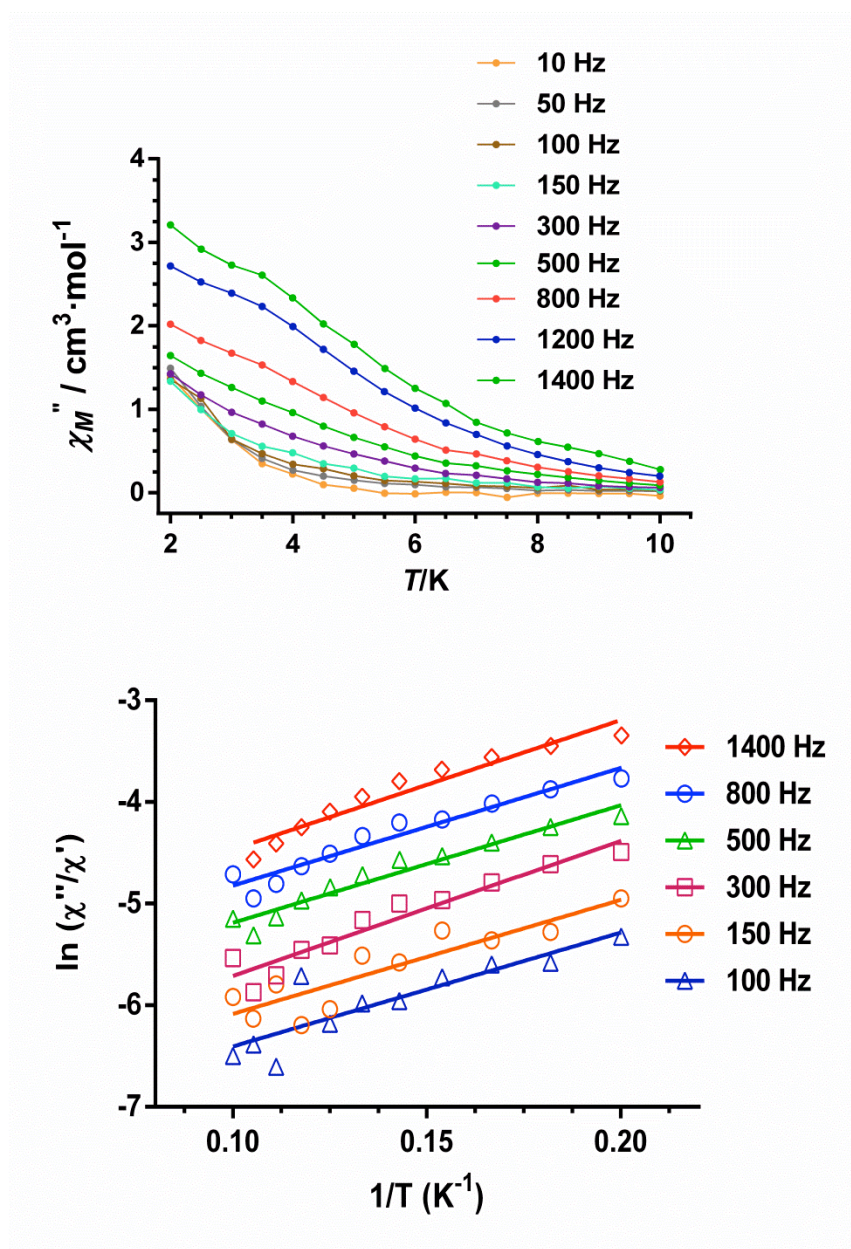


**Figure 23.** Temperature dependence of out-of-phase  $\chi_m''$  component of the ac susceptibility at 1000 Oe (top) applied dc field for complex **4**. Plots of  $\ln(\chi''/\chi')$  vs.  $1/T$  for **4**, the solid lines represent the fitting results (bottom).

## Conclusion

In summary, this work demonstrates the versatility of an aroylhydrazone based Schiff base ligand in assembling four  $\text{Dy}^{3+}$  complexes with  $\{\text{Dy}_2\}$ ,  $\{\text{Dy}_4\}$ ,  $\{\text{Dy}_6\}$  and  $\{\text{Dy}_{21}\}$  metallic skeletons. The change in nuclearity in these has been governed by the successive deprotonation of the ligand in combination with judicious choice of co-ligands. Although, compounds **1** and **2** project known structural topologies, **3** and **4** possess rare metallic skeletons in the pure lanthanide domain, equilateral triangle and single stranded nanowheel, respectively. To the best of our knowledge **4** is the first example of its kind with largest number of  $\text{Dy}^{3+}$  ions involved in the formation of a single-stranded nanowheel. Detailed magnetochemical analysis reveals the presence of frequency-dependent ac signals for **1**, **3** and **4** below 15 K without preponderant maxima in presence of zero dc field, affirming their slow magnetization relaxation characteristics, while compound **2** displays none.

## Experimental Section

Solvents and other general reagents used in this work were purified according to standard procedures.<sup>21</sup> Pyridine-2,6-dicarboxylic acid, sodium borohydride,  $\text{DyCl}_3 \cdot 6\text{H}_2\text{O}$  and  $\text{Dy}(\text{NO}_3)_3 \cdot 6\text{H}_2\text{O}$  were obtained from Sigma Aldrich Chemical Co. and were used as received.

Hydrazine hydrate (80%),  $\text{PBr}_3$ , 1,1,1-trifluoromethyl acetyl acetone, diethanolamine, 2-methyl-8-quinolinol, pivalic acid, triethyl amine and sodium sulfate (anhydrous) were obtained from S.D. Fine Chemicals, Mumbai, India. Methyl-6-(hydroxymethyl)picolinate,<sup>9g</sup> methyl-6-(bromomethyl)picolinate,<sup>[9g]</sup> *tert*-butyl phosphonic acid<sup>22</sup> and 8-hydroxyquinoline-2-carbaldehyde<sup>23</sup> were prepared according to literature procedures.

**Instrumentation.** Melting points were measured using a JSGW melting point apparatus and are uncorrected. IR spectra were recorded as KBr pellets on a Bruker Vector 22 FT IR spectrophotometer operating at 400–4000  $\text{cm}^{-1}$ . Elemental analyses of the compounds were obtained from Thermoquest CE instruments CHNS-O, EA/110 model. ESI–MS spectra were recorded on a MICROMASS QUATTRO II triple quadrupole mass spectrometer.  $^1\text{H}$  NMR spectra were recorded in  $\text{CDCl}_3$  and  $\text{CD}_3\text{OD}$  solutions on a JEOL JNM LAMBDA 400 model spectrometer operating at 500MHz. Chemical shifts are reported in parts per million (ppm) and are referenced with respect to internal tetramethylsilane ( $^1\text{H}$ ).

### Magnetic Measurements.

Magnetic data of **1-4** were recorded using a Quantum Design MPMS-5XL SQUID magnetometer. The polycrystalline samples were compacted and immobilized into cylindrical PTFE capsules. Dc data were acquired as a function of the magnetic field (0.1–5.0 T at 2.0 K) and temperature (2.0–290 K at 0.1 T). Ac data were measured in the frequency range 1–1000 Hz ( $T = 2.0\text{--}50$  K,  $B_{\text{ac}} = 3$  G). Data were corrected for the diamagnetic contributions of sample holder and compound (**1**:  $\chi_{\text{dia}} = -0.70 \times 10^{-3} \text{ cm}^3 \text{ mol}^{-1}$ , **2**:  $-1.07 \times 10^{-3} \text{ cm}^3 \text{ mol}^{-1}$ , **3**:  $-1.68 \times 10^{-3} \text{ cm}^3 \text{ mol}^{-1}$  and **4**:  $-5.3 \times 10^{-3} \text{ cm}^3 \text{ mol}^{-1}$ ).

**X-ray Crystallography.** The crystal data for the compounds have been collected on a Bruker SMART CCD diffractometer (MoK $\alpha$  radiation,  $\lambda = 0.71073 \text{ \AA}$ ). The program SMART<sup>23a</sup> was used for collecting frames of data, indexing reflections, and determining lattice parameters, SAINT<sup>23a</sup> for integration of the intensity of reflections and scaling, SADABS<sup>23b</sup> for absorption correction, and SHELXTL<sup>23c,23d</sup> for space group and structure determination and least-squares refinements on F<sup>2</sup>. The crystal structures were solved and refined by full-matrix least-squares methods against F<sup>2</sup> by using the program SHELXL-2014<sup>23e</sup> using Olex-2 software.<sup>23f</sup> All the non-hydrogen atoms were refined with anisotropic displacement parameters. Hydrogen positions were fixed at calculated positions and refined isotropically. The lattice solvent molecules of the complexes **3** and **4** could not be modeled satisfactorily due to the presence of severe disorder. Therefore, Olex-2 mask program has been performed to discard those disordered solvents molecules. The squeezed electron density of 373.65 and 902 corresponds to 4MeOH, H<sub>2</sub>O and 5CHCl<sub>3</sub> for **3**, and 7MeOH, 12CHCl<sub>3</sub> and 8H<sub>2</sub>O for **4**, respectively. In spite of our best efforts to obtain the best quality data, all the structures generate some alerts in check CIFs whose plausible origins are described in the Supporting Information. Crystallographic data (excluding structure factors) for the structures in this paper have been deposited with the Cambridge Crystallographic Data Centre as supplementary publication nos. CCDC 1514758–1514761. Copies of the data can be obtained, free of charge, on application to CCDC, 12 Union Road, Cambridge CB2 1EZ, UK, e-mail: data\_request@ccdc.cam.ac.uk, or fax: +44 1223 336033.

**Table 2.** Crystallographic details and structure refinement parameters of **1–4**.

	<b>1</b>	<b>2</b>	<b>3</b>	<b>4</b>
formula	C <sub>49</sub> N <sub>10</sub> O <sub>13</sub> ClDy <sub>2</sub> H <sub>59</sub>	C <sub>68</sub> H <sub>106</sub> N <sub>10</sub> O <sub>26</sub> Dy <sub>4</sub>	C <sub>164</sub> H <sub>174</sub> Cl <sub>14</sub> Dy <sub>12</sub> F <sub>18</sub> N <sub>30</sub> O <sub>71</sub> P <sub>2</sub>	C <sub>335</sub> H <sub>324</sub> Cl <sub>7</sub> Dy <sub>21</sub> F <sub>21</sub> N <sub>70</sub> O <sub>84</sub>
M / g mol <sup>-1</sup>	1356.51	2129.62	6551.57	10734.27
crystal system	Monoclinic	Triclinic	Trigonal	Triclinic
space group	<i>P</i> 2 <sub>1</sub> / <i>c</i>	<i>P</i> -1	<i>P</i> -3 <i>c</i> 1	<i>P</i> -1
<i>a</i> / Å	14.334(5)	12.700(5)	20.6099(9)	28.633(3)
<i>b</i> / Å	18.706(5)	14.162(5)	20.6099(9)	29.970(3)
<i>c</i> / Å	19.522(5)	14.694(5)	35.272(3)	33.075(3)
<i>α</i>	90°	62.162(5)°	90°	111.748(2)°
<i>β</i>	93.500(5)°	81.643(5)°	90°	97.588(2)°
<i>γ</i>	90°	63.369(5)°	120°	108.631(2)°
<i>V</i> / Å <sup>3</sup>	5225(3)	2082.2(13)	12975.1(15)	23949(4)
<i>Z</i>	4	1	2	2
<i>ρ</i> <sub>c</sub> / g cm <sup>-3</sup>	1.725	1.698	1.677	1.489
<i>μ</i> / mm <sup>-1</sup>	2.963	3.625	3.652	3.344
<i>F</i> (000)	2704.0	1056.0	6316.0	10380.0
crystal size / mm <sup>3</sup>	0.063 × 0.041 × 0.028	0.068 × 0.033 × 0.031	0.02 × 0.02 × 0.02	0.02 × 0.02 × 0.02
2 <i>θ</i> range	8.178 to 50.05	8.282 to 50.05	8.234 to 50.054	8.162 to 50.054
limiting indices	-17 ≤ <i>h</i> ≤ 17 -22 ≤ <i>k</i> ≤ 22 -23 ≤ <i>l</i> ≤ 23	-15 ≤ <i>h</i> ≤ 15 -16 ≤ <i>k</i> ≤ 16 -15 ≤ <i>l</i> ≤ 17	-27 ≤ <i>h</i> ≤ 27 -27 ≤ <i>k</i> ≤ 27 -46 ≤ <i>l</i> ≤ 46	-38 ≤ <i>h</i> ≤ 38 -40 ≤ <i>k</i> ≤ 40 -44 ≤ <i>l</i> ≤ 44
reflns collected	39487	22888	131670	754797
indep. reflns	9176 [R(int) = 0.0349]	7278 [R(int) = 0.0362]	7627 [R(int) = 0.1583]	84254 [R(int) = 0.1611]
completeness to <i>θ</i>	99.9 %	99.8 %	99.6 %	99.5 %
refinement method	Full-matrix least-squares on <i>F</i> <sup>2</sup>	Full-matrix least-squares on <i>F</i> <sup>2</sup>	Full-matrix least-squares on <i>F</i> <sup>2</sup>	Full-matrix least-squares on <i>F</i> <sup>2</sup>
data / restraints / parameters	9176 / 15 / 673	7278 / 19 / 451	7627 / 9 / 445	84254 / 73 / 4522
goodness-of-fit on <i>F</i> <sup>2</sup>	1.109	1.045	1.108	1.127
Final R indices [ <i>I</i> > 2 <i>θ</i> ( <i>I</i> )]	<i>R</i> <sub>1</sub> = 0.0470 <i>wR</i> <sub>2</sub> = 0.1059	<i>R</i> <sub>1</sub> = 0.0502 <i>wR</i> <sub>2</sub> = 0.1313	<i>R</i> <sub>1</sub> = 0.0592 <i>wR</i> <sub>2</sub> = 0.1599	<i>R</i> <sub>1</sub> = 0.0944 <i>wR</i> <sub>2</sub> = 0.2483
<i>R</i> indices (all data)	<i>R</i> <sub>1</sub> = 0.0559 <i>wR</i> <sub>2</sub> = 0.1113	<i>R</i> <sub>1</sub> = 0.0528 <i>wR</i> <sub>2</sub> = 0.1335	<i>R</i> <sub>1</sub> = 0.0920 <i>wR</i> <sub>2</sub> = 0.1736	<i>R</i> <sub>1</sub> = 0.1578 <i>wR</i> <sub>2</sub> = 0.2861

## Synthesis

### Methyl 6-((bis(2-hydroxyethyl)amino)methyl)picolinate

Triethylamine (4.2 mL, 31.9 mmol) was added dropwise to a solution of diethanolamine (0.959 g, 9.13 mmol) in THF (40 mL) at room temperature and stirred for 20 minutes. To this, methyl 6-(bromomethyl)picolinate (2.1 g, 9.13 mmol), dissolved in THF (40 mL) was added dropwise over a period of 25 minutes. The resultant colorless solution was stirred overnight at room temperature. A turbid solution that was formed was filtered and the filtrate was stripped off its solvent in vacuo to give oil like residue, which was re-dissolved in dichloromethane and washed with water. The organic portion was dried (sodium sulfate), filtered and evaporated affording yellow oil, which was shown to be the title compound. Yield: 2.61 g, 89.42 %. <sup>1</sup>H NMR (500 MHz, CDCl<sub>3</sub>, δ, ppm): 2.84 (t, 4H, -NCH<sub>2</sub>), 3.57 (t, 4H, -CH<sub>2</sub>O), 3.94 (s, 3H, OMe), 3.97 (s, 2H, NCH<sub>2</sub>), 5.28 (s, 1H, -OH), 7.43 (d, 1H, Py-H), 7.79 (t, 1H, Py-H), 8.01 (d, 1H, Py-H). ESI-MS, *m/z*: (M+H)<sup>+</sup>: 255.07. Anal. Calcd. for C<sub>12</sub>H<sub>18</sub>N<sub>2</sub>O<sub>4</sub> (254.28 g mol<sup>-1</sup>): C, 56.68; H, 7.13; N, 11.02 %. Found: C, 56.45; H, 7.28; N, 11.54 %.

### Methyl 6-((bis(2-hydroxyethyl)amino)methyl)picolinohydrazide

An ethanolic solution (15 mL) of hydrazine hydrate (1.48 g, 29.5 mmol) was added slowly to a solution of methyl 6-((bis(2-hydroxyethyl)amino)methyl)picolinate (1.5 g, 5.9 mmol) in ethanol (50 mL) at room temperature. The resulting light yellow solution was heated to reflux for 5 hours during which time the solution became turbid. At this stage, it was concentrated and kept in a refrigerator overnight, resulting in the formation of a white precipitate, which was filtered, washed twice with ethanol and dried. This was shown to be the title compound. Yield: 1.23 g, 83.1 %. Anal. Calcd. for C<sub>11</sub>H<sub>18</sub>N<sub>4</sub>O<sub>3</sub> (254.13 g mol<sup>-1</sup>): C, 51.96; H, 7.13; N, 22.03 %. Found: C,

52.44; H, 7.37; N, 22.45 %. Mp: 155 °C. <sup>1</sup>H NMR (500 MHz, CD<sub>3</sub>OD, δ, ppm): 2.73 (t, 4H, -NCH<sub>2</sub>), 3.61 (t, 4H, -CH<sub>2</sub>O), 3.95 (s, 2H, -NCH<sub>2</sub>), 7.69 (d, 2H, Py-H), 7.87 (t, 1H, Py-H). ESI-MS, *m/z*: (M+H)<sup>+</sup>: 255.11.

**6-((Bis(2-hydroxyethyl)amino)methyl)-N'-((8-hydroxyquinolin-2-yl)methylene)picolinohydrazide (LH<sub>4</sub>)**

To a stirred solution of methyl 6-((bis(2-hydroxyethyl)amino)methyl)picolinohydrazide (1 g, 3.93 mmol) in ethanol (40 mL), 8-hydroxyquinoline-2-carbaldehyde (0.68 g, 3.93 mmol) was added at room temperature and the resulting solution was refluxed for 3 hours to give an orange-yellow solution. The reaction mixture was allowed to come to room temperature and concentrated in vacuo before being kept in refrigerator overnight resulting in the formation of a yellow precipitate, which was filtered, washed 2-3 times with cold ethanol, diethyl ether and dried. This was shown to be the title compound. Yield: 1.21 g (74.6 %). Anal. Calcd. for C<sub>21</sub>H<sub>23</sub>N<sub>5</sub>O<sub>4</sub> (409.17 g mol<sup>-1</sup>): C, 61.60; H, 5.66; N, 17.10 %. Found: C, 60.92; H, 5.54; N, 16.84 %. Mp: 164 °C. <sup>1</sup>H NMR (500 MHz, CD<sub>3</sub>OD, δ, ppm): 2.81 (t, 4H, -NCH<sub>2</sub>), 3.70 (t, 4H, -CH<sub>2</sub>O), 4.00 (s, 2H, NCH<sub>2</sub>), 4.52 (br, 1H, CH<sub>2</sub>OH), 5.46 (s, 1H, -OH), 7.11 (d, 1H, Ar-H), 7.36 (d, 1H, Ar-H), 7.45 (t, 1H, Ar-H), 7.70 (d, 1H, Py-H), 7.96 (t, 1H, Py-H), 8.1 (d, 1H, Py-H), 8.26-8.29 (m, 2H, Ar-H), 8.68 (1H, imine-H). FT-IR (KBr), cm<sup>-1</sup>: 3397 (s), 3232 (s), 2954 (w), 2873 (w), 2807 (m), 1676 (s), 1589 (m), 1569 (m), 1504 (s), 1452 (m), 1464 (s), 1401 (s), 1267 (s), 1246 (m), 1212 (m), 1087 (s), 1035 (m), 994 (s), 946 (m), 922 (m), 871 (w), 845 (s), 764 (w), 721 (w), ESI-MS, *m/z*: (M+H)<sup>+</sup>: 410.13.

**Synthesis of [Dy<sub>2</sub>(LH<sub>2</sub>)<sub>2</sub>(μ<sub>2</sub>-η<sup>1</sup>η<sup>1</sup>Piv)]Cl·2MeOH·H<sub>2</sub>O (1)**

Solid DyCl<sub>3</sub>·6H<sub>2</sub>O (0.038g, 0.1 mmol) was added to a vigorously stirring solution of LH<sub>4</sub> (0.041g, 0.1 mmol) in methanol (30 mL) at room temperature to give a dark red solution. After stirring for 10 minutes, triethylamine (0.04 mL, 0.3 mmol) was added drop wise during which solution lightened slightly. The reaction mixture was kept under stirring for 15 minutes. At this stage, pivalic acid (0.01 mL, 0.1 mmol) was added dropwise and the mixture was stirred overnight at room temperature. All the volatiles were removed from the reaction mixture in vacuo affording a dark red residue, which was washed twice with diethyl ether, dried and dissolved in methanol. Diethyl ether was allowed to slowly diffuse into this solution. X-ray quality crystals were obtained over a period of seven days. Yield: 0.056 g, 41.2% (based on Dy<sup>3+</sup>). Mp: >250 °C (d). IR (KBr), cm<sup>-1</sup>: 3368 (br), 2960 (m), 1607 (w), 1588 (m), 1559 (s), 1518 (s), 1500 (s), 1451 (s), 1426 (s), 1372 (s), 1308 (s), 1274 (s), 1228 (m), 1186 (m), 1043 (s), 1013 (m), 960 (m), 844 (w), 793 (w), 768 (w), 754 (w), 737 (w), 692 (w). Anal. Calcd. for C<sub>49</sub>H<sub>59</sub>ClDy<sub>2</sub>N<sub>10</sub>O<sub>13</sub> (1356.52 g mol<sup>-1</sup>): C, 43.39; H, 4.38; N, 10.33 %. Found: C, 43.67; H, 4.19; N, 10.52 %. ESI-MS *m/z*, ion: 1139.191 (C<sub>47</sub>H<sub>51</sub>Dy<sub>2</sub>N<sub>10</sub>O<sub>10</sub>- Piv - H<sup>+</sup>)<sup>+</sup>.

**Synthesis of [Dy<sub>4</sub>(LH)<sub>2</sub>(μ<sub>3</sub>-OH)<sub>2</sub>(Piv)<sub>4</sub>(MeOH)<sub>2</sub>]·4MeOH·2H<sub>2</sub>O (2)**

Dy(NO<sub>3</sub>)<sub>3</sub>·5H<sub>2</sub>O (0.087 g, 0.2 mmol) was charged into a methanolic solution (40 mL) of LH<sub>4</sub>(0.041 g, 0.1 mmol) followed by addition of Et<sub>3</sub>N (0.04 mL, 0.3 mmol) at room temperature. The resulting dark red solution was stirred for 20 minutes. At this stage, pivalic acid (0.02 g, 0.2 mmol) was added dropwise and the reaction mixture was stirred further for 10 minutes. Then, Et<sub>3</sub>N (0.026 mL, 0.2 mmol) was added and the reaction mixture was heated under reflux for 3 hours. The red solution was removed off its volatiles in vacuo to afford a reddish residue, which

was washed 2–3 times with diethyl ether and dried before being dissolved in MeOH/CHCl<sub>3</sub> (1:1, v/v) and kept for crystallization at room temperature. Block-shaped crystals, suitable for X-ray diffraction were obtained over a period of 12 days. Yield: 0.069 g, 32.7 % (based on Dy<sup>3+</sup>). Mp: >250 °C (d). IR (KBr), cm<sup>-1</sup>: 3405 (br), 2957 (m), 2850 (w), 2678 (w), 1550 (s), 1518 (s), 1500 (s), 1483 (s), 1451 (s), 1413 (s), 1383 (s), 1339 (s), 1307 (s), 1224 (m), 1186 (m), 1074 (s), 1014(w), 956 (m), 892 (m), 841 (w), 786 (w), 766 (w), 743 (w), 691 (w), 646 (w). Anal. Calcd. for C<sub>68</sub>H<sub>106</sub>Dy<sub>4</sub>N<sub>10</sub>O<sub>26</sub> (2129.63 g mol<sup>-1</sup>): C, 38.35; H, 5.02; N, 6.58 %. Found C, 38.71; H, 4.93; N, 6.28 %. ESI-MS *m/z*, ion: 1902.299 [C<sub>64</sub>H<sub>86</sub>Dy<sub>4</sub>N<sub>10</sub>O<sub>20</sub> - 2MeOH + H<sup>+</sup>]<sup>+</sup>.

### Synthesis of [Dy<sub>6</sub>(LH<sub>2</sub>)<sub>3</sub>(tfa)<sub>3</sub>(O<sub>3</sub>P<sup>t</sup>Bu)(Cl)<sub>3</sub>]Cl<sub>4</sub>·15.5H<sub>2</sub>O·4MeOH·5CHCl<sub>3</sub> (3)

DyCl<sub>3</sub>·6H<sub>2</sub>O (0.075 g, 0.2 mmol) was added to a solution of LH<sub>4</sub> (0.041g, 0.1 mmol) dissolved in methanol. This was followed by the addition of triethylamine (0.066 mL, 0.5 mmol). The reaction mixture was stirred for 15 minutes at room temperature. At this stage, 1,1,1-trifluoromethyl acetylacetone (tfa; 0.015 g, 0.1 mmol) was added and the stirring resumed for a further period of 15 minutes at room temperature. Finally, tert-butyl phosphonic acid (0.033, 0.033 mmol) dissolved in methanol was added slowly and the reaction mixture was continued under stirring overnight affording a brick-red colored solution which was removed off its volatiles in vacuo to afford a semi-solid mass which was washed twice with diethyl ether before being dissolved in methanol. Diethyl ether was allowed to slowly diffuse into this solution. Crystals suitable for X-ray diffraction were obtained over a period of 15 days. Yield: 0.043 g, 31.1 % (based on the Dy<sup>3+</sup>). Mp: >250 °C (d). IR (KBr), cm<sup>-1</sup>: 3401 (br), 2863 (m), 1633 (s), 1591(m), 1507 (s), 1452 (s), 1376 (s), 1336 (s), 1223 (s), 1184 (s), 1139 (s), 1106 (s), 1009 (m), 966 (m), 854 (m), 842 (w), 762 (m), 741 (m), 725 (s), 691 (w), 656 (w), 560 (w), 487 (w), 424

(w). Anal. Calcd. for  $C_{91}H_{133}Cl_{22}Dy_6F_9N_{15}O_{40.5}P$  ( $4056.02 \text{ g mol}^{-1}$ ): C, 27.04; H, 3.32; N, 5.2 %. Found: C, 27.81; H, 3.59; N, 5.18 %. ESI-MS  $m/z$ , ion:  $1474.066 [C_{82}H_{81}Cl_3Dy_6F_9N_{15}O_{21}P - 2Cl^- + 3H_2O + 2MeOH - 4H^+]^{2+}$ .

#### Synthesis of $[Dy_{21}(L)_7(LH)_7(tfa)_7]Cl_7 \cdot 15H_2O \cdot 7MeOH \cdot 12CHCl_3$ (4)

To a stirred solution of  $LH_4$  (0.041 g, 0.1 mmol) in MeOH,  $DyCl_3 \cdot 6H_2O$  (0.056 g, 0.15 mmol), was added at room temperature. The resulting red solution was stirred for 15 minutes. Then, trimethylamine (0.052 mL, 0.4 mmol) was added dropwise and the reaction mixture was continued under stirring for a further period of 20 minutes. At this stage, 1,1,1-trifluoro acetyl acetone (0.007 g, 0.05 mmol) was added dropwise to the reaction mixture to afford an orange-red solution which was stirred overnight at room temperature. This was removed off its volatiles to afford a solid mass that was washed 2–3 times with diethyl ether and dried before dissolving in MeOH/ $CHCl_3$  (1:1 v/v). Diethyl ether was allowed to slowly diffuse into this solution. Block-shaped crystals suitable for X-ray diffraction were obtained over a period of 4 days. Yield: 0.032 g, 35.9 % (based on  $Dy^{3+}$ ). Mp:  $>250 \text{ }^\circ\text{C}$  (d). IR (KBr),  $\text{cm}^{-1}$ : 3407 (br), 2862 (br), 1634 (s), 1587 (m), 1548 (s), 1535 (s), 1502 (s), 1450 (s), 1432 (m), 1377 (s), 1309 (w), 1291 (s), 1219 (s), 1183 (s), 1135 (s), 1103 (s), 1089 (s), 1007 (br), 965 (s), 931 (s), 891 (m), 852 (m), 761 (s), 740 (m), 724 (s), 687 (s), 590 (w), 558 (m), 488 (w). Anal. Calcd. for  $C_{354}H_{380}Cl_{42}Dy_{21}F_{21}N_{70}O_{99}$  ( $12499.69 \text{ g mol}^{-1}$ ): C, 34.02; H, 3.06; N, 7.84 %. Found: C, 34.99; H, 3.82; N, 8.37 %.

**Supporting Information:** List of bond lengths and bond angles of **1–4** (Table S1–S4), ESI-MS of **2** and **3** (Figure S1, S2), supramolecular interaction of **1–4** (Figure S3, S4), hydrogen bond parameter table (Table S5), temperature dependence in phase and out of phase susceptibility of **4** in absence and presence of dc fields (Figure S5–S7), exploratory magnetochemical modeling for **1** and **2**, CheckCIF alert responses.

**Acknowledgement:** We thank the Department of Science and Technology (DST), India, for financial support, including support for a single-crystal CCD X-ray diffractometer facility at IIT-Kanpur. V.C. is grateful to the DST for a J. C. Bose fellowship. S.B. thanks Council of Scientific and Industrial Research, India for Senior Research Fellowship. Financial support from Ministerio de Economía y Competitividad (MINECO) for Project CTQ2014-56312-P, the Junta de Andalucía (FQM-195 and the Project of excellence P11-FQM-7756) and the University of Granada are gratefully acknowledged by E.C. and J.M.H.

## References

- [1] a) R. Sessoli, D. Gatteschi, A. Caneschi, M. A. Novak, *Nature* **1993**, *365*, 141–143; b) R. Sessoli, L. Hui, A. R. Schake, S. Wang, J. B. Vincent, K. Folting, D. Gatteschi, G. Christou, *J. Am. Chem. Soc.* **1993**, *115*, 1804–1816.
- [2] a) J. Liu, Y.-C. Chen, J.-L. Liu, V. Vieru, L. Ungur, J.-H. Jia, L. F. Chibotaru, Y. Lan, W. Wernsdorfer, S. Gao, X.-M. Chen, M. L. Tong, *J. Am. Chem. Soc.* **2016**, *138*, 5441–5450; b) Y. C. Chen, J. L. Liu, L. Ungur, J. Liu, Q.-W. Li, L.-F. Wang, Z. Ping, L. F. Chibotaru, X.-M. Chen, M. L. Tong, *J. Am. Chem. Soc.* **2016**, *138*, 2829–2837; c) R. Sato, K. Suzuki, T. Minato,

M. Shinoe, K. Yamaguchi, N. Mizuno, *Chem. Commun.* **2015**, *51*, 4081–4084; d) H. Ke, G.-F. Xu, Y.-N. Guo, P. Gamez, C. M. Beavers, S. J. Teat, J. Tang, *Chem. Commun.* **2010**, *46*, 6057–6059; e) S. Das, A. Dey, S. Kundu, S. Biswas, R. S. Narayanan, S. T. Padilla, G. Lorusso, M. Evangelisti, E. Colacio, V. Chandrasekhar, *Chem. Eur. J.* **2015**, *21*, 16955–16967; f) X. L. Li, J. Wu, J. Tang, B. L. Guennic, W. Shi, P. Cheng, *Chem. Commun.* **2016**, *52*, 9570–9573; g) S. Biswas, S. Das, S. Hossain, A. K. Bar, J.-P. Sutter, V. Chandrasekhar, *Eur. J. Inorg. Chem.* **2016**, 4683–4692.

[3] a) S. K. Langley, D. P. Wielechowski, B. Moubaraki, K. S. Murray, *Chem. Commun.* **2016**, *52*, 10976–10979; b) I. A. Kühne, V. Mereacre, C. E. Ansona, A. K. Powell, *Chem. Commun.* **2016**, *52*, 1021–1024; c) E. Colacio, J. Ruiz, E. Ruiz, E. Cremades, J. Krzystek, S. Carretta, J. Cano, T. Guidi, W. Wernsdorfer, E. K. Brechin, *Angew. Chem. Int. Ed.* **2013**, *52*, 9130–9134; d) X.-Q. Song, P.-P. Liu, Y.-A. Liu, J.-J. Zhou, X.-L. Wang, *Dalton Trans.* **2016**, *45*, 8154–8163; e) H. Li, W. Shi, Z. Niu, J.-M. Zhou, G. Xiong, L.-L. Li, P. Cheng, *Dalton Trans.* **2015**, *44*, 468–471; f) I. Oyarzabal, B. Artetxe, A. R.-Diéguez, J. Á. García, J. M. Seco, E. Colacio, *Dalton Trans.* **2016**, *45*, 9712–9726; g) P. Bag, A. Chakraborty, G. Rogez, V. Chandrasekhar, *Inorg. Chem.* **2014**, *53*, 6524–6533; h) V. Chandrasekhar, P. Bag, M. Speldrich, J. van Leusen, P. Kögerler, *Inorg. Chem.* **2013**, *52*, 5035–5044; i) S. Biswas, J. Goura, S. Das, C. V. Topping, J. Brambleby, P. A. Goddard, V. Chandrasekhar, *Inorg. Chem.* **2016**, *55*, 8422–8436; j) S. She, Y. Li, W. Li, *Dalton Trans.* **2016**, *45*, 10830–10835; k) S. G. Baca, J. van Leusen, M. Speldrich, P. Kögerler, *Inorg. Chem. Front.* **2016**, *3*, 1071–1075; l) H. L. C. Feltham, S. Dhers, M. Rouzières, R. Clérac, A. K. Powell, S. Brooker, *Inorg. Chem. Front.* **2015**, *2*, 982–990; m) P. Richardson, D. I. Alexandropoulos, L. C. -Silva, G. Lorusso, M. Evangelisti, J. Tang, T. C. Stamatatos,

*Inorg. Chem. Front.* **2015**, *2*, 945–948; n) A. Amjad, A. M. Madalan, M. Andruh, A. Caneschi, L. Sorace, *Chem. Eur. J.* **2016**, *22*, 12849–12858; o) M. H. Ojea, V. A. Milway, G. Velmurugan, L. H. Thomas, S. J. Coles, C. Wilso, W. Wernsdorfer, G. Rajaraman, M. Murri, *Chem. Eur. J.* **2016**, *22*, 12839–12848; p) S. Biswas, H. S. Jena, A. Adhikary, S. Konar, *Inorg. Chem.* **2014**, *53*, 3926–3928.

[4] a) V. Chandrasekhar, A. Dey A. J. Mota, E. Colacio, *Inorg. Chem.* **2013**, *52*, 4554–4561; b) D. W. Boukhvalov, V. V. Dobrovitski, P. Kögerler, M. Al-Saqer, M. Katsnelson, A. I. Lichtenstein, B. N. Harmon, *Inorg. Chem.* **2010**, *49*, 10902–10906; c) F. Shao, B. Cahier, N. Guihery, E. Riviere, A. L. Barra, Y. Lan, W. Wernsdorfer, V. E. Campbell, T. Mallah, *Chem. Commun.* **2015**, *51*, 16475–16478; d) A. K. Bar, C. Pichon, N. Gogoi, C. Duhayon, S. Ramaseshac, J. P. Sutter, *Chem. Commun.* **2015**, *51*, 3616–3619; e) R. Sato, K. Suzuki, T. Minato, M. Shinoe, K. Yamaguchi, N. Mizuno, *Chem. Commun.* **2015**, *51*, 4081–4084; f) A. K. Bar, C. Pichona, J. P. Sutter, *Coord. Chem. Rev.* **2016**, *308*, 346–380; g) A. S. Dinca, N. Candu, S. Shova, F. Lloret, M. Julve, V. I. Parvulescu, M. Andruh, *RSC Adv.* **2016**, *6*, 86569–86574; h) P. S. Perlepe, L. C. Silva, V. Bekiari, K. J. Gagnon, S. J. Teat, A. Escuere, T. C. Stamatatos, *Dalton Trans.* **2016**, *45*, 10256–10270; i) K. I. Alexopoulou, A. Terzis, C. P. Raptopoulou, V. Psycharis, A. Escuer, S. P. Perlepes, *Inorg. Chem.* **2015**, *54*, 5615–5617.

[5] a) S. Biswas, S. Das, J. V. Leusen, P. Kögerler, V. Chandrasekhar, *Dalton Trans.* **2015**, *44*, 19282–19293; b) J. Goura, J. P. S. Walsh, F. Tuna, V. Chandrasekhar, *Inorg. Chem.* **2014**, *53*, 3385–3391; c) S. Biswas, A. Mondal, S. Konar, *Inorg. Chem.* **2016**, *55*, 2085–2090; d) A. Mondal, V. S. Parmar, S. Biswas, S. Konar, *Dalton Trans.* **2016**, *45*, 4548–4557; e) A. J.

Calahorro, I. Oyarzabal, B. Fernández, J. M. Seco, T. Tian, D. F.-Jimenez, E. Colacio, A. R. - Diéguez, *Dalton Trans.* **2016**, *45*, 591–598; f) S. Biswas, S. Das, G. Rogez, V. Chandrasekhar, *Eur. J. Inorg. Chem.* **2016**, 3322–3329; g) G. Brunet, F. Habib, I. Korobkov, M. Murugesu, *Inorg. Chem.* **2015**, *54*, 6195–6202; h) L. Zhang, P. Zhang, L. Zhao, J. Wu, M. Guoa, J. Tang, *Dalton Trans.* **2016**, *45*, 10556–10562; i) S. Das, A. Dey, S. Biswas, E. Colacio, V. Chandrasekhar, *Inorg. Chem.* **2014**, *53*, 3417–3426; j) S. Das, S. Hossain, A. Dey, S. Biswas, J.-P. Sutter, V. Chandrasekhar, *Inorg. Chem.* **2014**, *53*, 5020–5028; k) S. G. Reis, M. Briganti, D. O. T. A. Martins, H. Akpinar, S. Calancea, G. P. Guedes, S. Soriano, M. Andruh, R. A. A. Cassaro, P. M. Lahti, F. Totti, Maria G. F. Vaz, *Dalton Trans.* **2016**, *45*, 2936–2944; l) M. Andruh, *Dalton Trans.* **2015**, *44*, 16633–16653; m) E. C. Mazarakioti, L. Cunha-Silva, V. Bekiari, A. Escuer, T. C. Stamatatos, *RSC Adv.* **2015**, *5*, 92534–92538; n) Z.-M. Zhang, K. H. Zangana, A. K. Kostopoulos, M.-L. Tong, R. E. P. Winpenny, *Dalton Trans.* **2016**, *45*, 9041–9044; o) E. M. Pineda, G. Lorusso, K. H. Zangana, E. Palacios, J. Schnack, M. Evangelisti, R. E. P. Winpenny, E. J. L. McInnes, *Chem. Sci.* **2016**, *7*, 4891–4895; p) M. Gregson, N. F. Chilton, A.-M. Ariciu, F. Tuna, I. F. Crowe, W. Lewis, A. J. Blake, D. Collison, E. J. L. McInnes, R. E. P. Winpenny, S. T. Liddle, *Chem. Sci.* **2016**, *7*, 155–165; q) C. Das, S. Vaidya, T. Gupta, J. M. Frost, M. Righi, E. K. Brechin, M. Affronte, G. Rajaraman, M. Shanmugam, *Chem. Eur. J.* **2015**, *21*, 15639–15650; r) S. K. Singh, M. F. Beg, G. Rajaraman, *Chem. Eur. J.* **2016**, *22*, 672–680; s) S. K. Gupta, A. Dar, T. Rajeshkumar, S. Kuppaswamy, S. K. Langley, K. S. Murray, G. Rajaraman, R. Murugavel, *Dalton Trans.* **2015**, *44*, 5961–5965; t) S. K. Gupta, T. Rajeshkumar, G. Rajaraman, R. Murugavel, *Chem. Sci.* **2016**, *7*, 5181–5191.

[6] a) S. K. Langley, D. P. Wielechowski, V. Vieru, N. F. Chilton, B. Moubaraki, L. F. Chibotaru, K. S. Murray, *Chem. Commun.* **2015**, *51*, 2044–2047; b) Y. Zheng, Y.-Y. Pan, Y.-P. Ren, L.-S. Long, R.-B. Huang, L.-S. Zheng, *Chem. Commun.* **2014**, *50*, 14728–14731; c) K. S. Pedersen, J. Bendix, R. Clérac, *Chem. Commun.* **2014**, *50*, 4396–4415; d) X. Y. Wang, C. Avendanoa, K. R. Dunbar, *Chem. Soc. Rev.* **2011**, *40*, 3213–3238.

[7] a) L. Chatelain, F. Tuna, J. Pe'cautab, M. Mazzant, *Chem. Commun.* **2015**, *51*, 11309–11312; b) V. Mougel, L. Chatelain, J. Hermle, R. Caciuffo, E. Colineau, F. Tuna, N. Magnani, A. de Geyer, J. Pecaut, M. Mazzanti, *Angew. Chem., Int. Ed.* **2014**, *53*, 819–823; c) F. Moro, D. P. Mills, S. T. Liddle, J. Slagereen, *Angew. Chem., Int. Ed.* **2013**, *52*, 1–5; d) M. A. Antunes, L. C. J. Pereira, I. C. Santos, M. Mazzanti, J. Marçalo, M. Almeida, *Inorg. Chem.* **2011**, *50*, 9915–9917; e) J. T. Coutinho, M. A. Antunes, L. C. J. Pereira, H. Bolvin, J. Marçalo, M. Mazzanti, M. Almeida, *Dalton Trans.* **2012**, *41*, 13568–13571; f) N. Magnani, E. Colineau, R. Eloirdi, J.-C. Griveau, R. Caciuffo, S. M. Cornet, I. May, C. A. Sharrad, D. Collison, R. E. P. Winpenny, *Phys. Rev. Lett.* **2010**, *104*, 197202–197208.

[8] a) R. Sessoli, D. Gatteschi, A. Caneschi, M. A. Novak, *Nature* **1993**, *365*, 141 – 143; b) D. Gatteschi, R. Sessoli, J. Villain, *Molecular Nanomagnets*, Oxford Univ. Press, **2006**.

[9] a) S. Das, A. Dey, S. Biswas E. Colacio, V. Chandrasekhar, *Inorg. Chem.* **2014**, *53*, 3417–3426; b) L. Zhang, P. Zhang, L. Zhao, S. -Y. Lin, S. Xue J. Tang, Z. Liu, *Eur. J. Inorg. Chem.* **2013**, 1351–1357; c) R. J. Blagg, L. Ungur, F. Tuna, J. Speak, P. Comar, D. Collison, W. Wernsdorfer, E. J. L. McInnes, R. E. P. Winpenny, *Nature Chem.* **2013**, *5*, 673–678; d) V.

Chandrasekhar, P. Bag, M. Speldrich, J. V. Leusen, P. Kögerler, *Inorg. Chem.* **2013**, *52*, 5035–5044; e) J. Wu, L. Zhao, M. Guo, J. Tang, *Chem. Commun.* **2015**, *51*, 17317–17320; f) S. Biswas, S. Das, J. V. Leusen, P. Kögerler, V. Chandrasekhar, *Eur. J. Inorg. Chem.* **2014**, *25*, 4159–4167; g) V. Chandrasekhar, S. Das, A. Dey, S. Hossain, J.-P. Sutter, *Inorg. Chem.* **2013**, *52*, 11956–11965.

[10] a) P. Zhang, L. Zhang, S. -Y. Lin, J. Tang, *Inorg. Chem.* **2013**, *52*, 6595–6602; b) N. Guo, X. -H. Chen, S. Xue, J. Tang, *Inorg. Chem.* **2012**, *51*, 4035–4042; c) G. M. Liang, Q. -L. Ni, H. -H. Zou, L. -C. Gui, X. -J. Wang, *Chem. Commun.* **2016**, *52*, 5293–5296; d) N. J. Yutronkie, I. A. Kühne, I. Korobkov, J. L. Brusso, M. Murugesu, *Chem. Commun.* **2016**, *52*, 677–680; e) A. A. Athanasopoulou, M. Pilkington, C. P. Raptopoulou, A. Escuer, T. C. Stamatatos, *Chem. Commun.* **2014**, *50*, 14942–14945; f) H. Tian, L. Zhao, H. Lin, J. Tang, G. Li, *Chem. Eur. J.* **2013**, *19*, 13235 –13241; g) C. Aronica, G. Chastanet, G. Pilet, B. L. Guennic, V. Robert, W. Wernsdorfer, D. Luneau, *Inorg. Chem.* **2007**, *46*, 6108–6119.

[11] a) H. Tian, M. Wang, L. Zhao, Y. Guo, J. Tang, Z. Liu, *Chem. Eur. J.* **2012**, *18*, 442–445; b) S. -Y. Lin, W. Wernsdorfer, L. Ungur, A. K. Powell, Y. -N. Guo, J. Tang, L. Zhao, L. F. Chibotaru, Zhang, H. -J. *Angew. Chem., Int. Ed.* **2012**, *51*, 12767–12771; c) Y. -N. Guo, X. -H. Chen, S. Xue, J. Tang, *Inorg. Chem.* **2012**, *51*, 4035–4042; d) I. J. Hewitt, J. Tang, N. T. Madhu, C. E. Y. Anson, J. Lan, M. Luzon, R. Etienne, A. K. Sessoli, *Angew. Chem., Int. Ed.* **2010**, *49*, 6352–6356; e) H. Ke, L. Zhao, Y. Guo, J. Tang, *Eur. J. Inorg. Chem.* **2011**, 4153–4156; e) S. Liao, X. Yang, R. A. Jones, *Cryst. Growth Des.* **2012**, *12*, 970–974; f) X. L. Li, H. Li, D. -M.

Chen, C. Wang, J. Wu, J. Tang, W. Shi, P. Cheng, *Dalton Trans.* **2015**, *44*, 20316–20320; g) B. Joarder, S. Mukherjee, S. Xue, J. Tang, S. K. Ghosh, *Inorg. Chem.* **2014**, *53*, 7554–7560.

[12] a) I. L. Malaestean, A. Ellern, S. Baca, P. Kögerler, *Chem. Commun.* **2012**, *48*, 1499–1503; b) L. X. Chang, G. Xiong, L. Wang, P. Cheng B. Zhao, *Chem. Commun.* **2013**, *49*, 1055–1057; c) X. J. Gu, D. F. Xue, *Inorg. Chem.* **2007**, *46*, 3212–3216; d) X. –Y. Zheng, J. –B. Peng, X. J. Kong, L. –S. Long, L. –S. Zheng, *Inorg. Chem. Front.* **2016**, *3*, 320–325; e) M. Romanelli, G. A. Kumar, T. J. Emge, R. E. Riman, J. G. Brennan, *Angew. Chem. Int. Ed.* **2008**, *47*, 6049–6051; f) X. Gu, R. Clérac, A. Hourri, D. Xue, *Inorg. Chim. Acta* **2008**, *361*, 3873–3876.

[13] K. Wang, Z.-L. Chen, H.-H. Zou, K. Hu, H.-Y. Li, Z. Zhang, W.-Y. Sun, F. P. Liang, *Chem. Commun.* **2016**, *52*, 8297–8300.

[14] H. Lueken, *Magnetochemie*, Teubner, Stuttgart, **1999**.

[15] a) M. Speldrich, H. Schilder, H. Lueken, P. Kögerler *Isr. J. Chem.* **2011**, *51*, 215–227; b) J. van Leusen, M. Speldrich, H. Schilder, P. Kögerler, *Coord. Chem. Rev.* **2015**, *289–290*, 137–148.

[16] (a) M. Llunell, D. Casanova, J. Cirera, P. Alemany, S. Alvarez, *SHAPE 2.0*, Universitat de Barcelona, Barcelona, **2010**; (b) S. Alvarez, P. Alemany, D. Casanova, J. Cirera, M. Llunell, D. Avnir, *Coord. Chem. Rev.* **2005**, *249*, 1693–1708.

[17] (a) J. S. Griffith, *The Theory of Transition-Metal Ions*, Cambridge University Press, Cambridge, **1971**; (b) E. U. Condon, G. H. Shortley, *The Theory of Atomic Spectra*, Cambridge University Press, Cambridge, **1951**.

[18] K. S. Cole, R. H. Cole, *J. Chem. Phys.* **1941**, *9*, 341–351.

[19] a) D. N. Woodruff, R.E.P. Winpenny, R.A. Layfield, *Chem. Rev.* **2013**, *113*, 5110–5148; b) P. Zhang, Y. -N. Guo, J. Tang, *Coord. Chem. Rev.* **2013**, *257*, 1728–1735; c) R. A. Layfield and M. Murugesu (eds.), *Lanthanides and Actinides in Molecular Magnetism*, Wiley-VCH, Weinheim, **2015**; d) J. Tang, P. Zhang, *Lanthanide Single Molecule Magnets*, Springer, Berlin, **2015**.

[20] a) J. Ruiz, A. J. Mota, A. Rodríguez-Diéguez, S. Titos, J. M. Herrera, E. Ruiz, E. Cremades, J. P. Costes, E. Colacio, *Chem. Commun.* **2012**, *48*, 7916–7918; b) H. L. C. Feltham, Y. Lan, F. Klöwer, L. Ungur, L. F. Chibotaru, A. K. Powell, S. Brooker, *Chem. Eur. J.* **2011**, *17*, 4362–4365; c) Y. Bi, Y.-N. Guo, L. Zhao, Y. Guo, S.-Y. Lin, S. D. Jiang, J. Tang, B. W. Wang, S. Gao, *Chem. Eur. J.* **2011**, *17*, 12476–12481 and references therein.

[21] a) *Vogel's Textbook of Practical Organic Chemistry*, 5th ed.; B. S. Furniss, A. J. Hannaford, P. W. G. Smith, A. R. Tatchell, Eds., ELBS, Longman: London, **1989**; b) D. B. G. Williams, M. Lawton, *J. Org. Chem.* **2010**, *75*, 8351–8354; c) X. Zeng, D. Coquiére, A. Alenda, E. Garrier, T. Prangé, Y. Li, O.Reinaud, I. Jabin, *Chem. Eur. J.* **2006**, *12*, 6393–6402.

[22] P. C. Crofts, G. M. Kosolapoff, *J. Am. Chem. Soc.* **1953**, *75*, 3379–3383.

[23] a) *SMART & SAINT Software Reference manuals*, Version 6.45; Bruker Analytical X-ray Systems, Inc.: Madison, WI, **2003**; b) G. M. Sheldrick, SADABS, *a software for empirical absorption correction*, Ver. 2.05; University of Göttingen: Göttingen, Germany, **2002**; c) *SHELXTL Reference Manual*, Ver. 6.1; Bruker Analytical X-ray Systems, Inc.: Madison, WI, **2000**; d) G. M. Sheldrick, *SHELXTL*, Ver. 6.12; Bruker AXS Inc.: WI. Madison, **2001**; e) G. M. Sheldrick, *Acta Crystallogr. Sect. A: Fundam. Crystallogr.* **2008**, *64*, 112–122; f) O. V. Dolomanov, L. J. Bourhis, R. J. Gildea, J. A. K. Howard, H. Puschmann, *J. Appl. Crystallogr.* **2009**, *42*, 339–341; g) K. Brandenburg, *Diamond*, Ver. 3.1e; Crystal Impact GbR: Bonn, Germany, **2005**.

## Graphical Abstract

Utilization of a multidentate flexible aroyl hydrazine-based Schiff base ligand, 6-((bis(2-hydroxyethyl)amino)methyl)-*N'*-((8-hydroxyquinolin-2-yl)methylene)picolinohydrazide leads to formation of four complexes with  $\{Dy_2\}$ ,  $\{Dy_4\}$ ,  $\{Dy_6\}$  and  $\{Dy_{21}\}$  metallic cores. Nuclearity here is controlled by the successive deprotonation of the ligand in combination with judicious choice of co-ligands. Detailed static and dynamic magnetic properties of all the complexes reveal SMM characteristics for the  $\{Dy_2\}$ ,  $\{Dy_6\}$  and  $\{Dy_{21}\}$  complexes.

